Title

Pnrc2 promotes rapid mRNA decay and coordinately supports early development with P-body factors Ddx6 and Ddx61

Running title

Pnrc2, P-bodies, and development

Authors

Gallagher, Thomas L.[1,2,‡]; Blatnik, Monica C.[1,2,3,*]; Austin, Clare C.[1,2]; Thompson, Kathryn G.[1,2]; Pvirre, Danielle M.[1]; Morgan, Angelina[1]; Kearse, Michael G.[2,4]; Amacher, Sharon L.[1,2,3,5‡]

1 Department of Molecular Genetics, The Ohio State University, Columbus, OH, 43210, USA

2 Center for RNA Biology, The Ohio State University, Columbus, OH, 43210, USA

3 Interdisciplinary Graduate Program in Molecular, Cellular and Developmental Biology, The Ohio State University, Columbus, OH, 43210, USA

4 Department of Biological Chemistry and Pharmacology, The Ohio State University, Columbus, OH, 43210, USA

5 Center for Muscle Health and Neuromuscular Disorders, The Ohio State University, Columbus, OH, 43210, USA.

*Present address: Oberlin College of Arts and Sciences, 38 E. College St., Oberlin, OH, 44074, USA.

‡Authors for correspondence (gallagher.184@osu.edu and amacher.6@osu.edu)

Keywords

somitogenesis, oscillatory gene expression, P-bodies, translational regulation, deadenylation

Abstract

Somitogenesis, the sequential segmentation of vertebrate embryonic mesoderm, is controlled by the segmentation clock, a molecular oscillator that controls periodic gene expression in unsegmented mesoderm and is regulated by a negative feedback loop driven by Hes/Her transcriptional repressors. In zebrafish, Pnrc2 is required for decay of *her1* transcript and additional oscillatory gene transcripts. Despite accumulation of numerous mRNAs including those encoding key developmental regulators, overt embryonic phenotypes are absent in *pnrc2* mutants. Our previous work suggested that accumulated mRNAs are not translated in *pnrc2* mutants, though the underlying mechanism(s) was unknown. We show here that many overexpressed transcripts in *pnrc2* mutants have shortened poly(A) tails and are disengaged from ribosomes, and that deadenylation inhibition leads to somite defects in *pnrc2* mutants. In contrast, transcripts encoding the P-body protein, Ddx61, are both overexpressed and engaged with ribosomes, leading to an increase in Ddx61 protein. Co-depletion of Ddx61 and its ohnolog Ddx6 enhances *her1* accumulation and later leads to strong morphological defects in *pnrc2* mutants. Together, our results show that multiple post-transcriptional mechanisms ensure proper translation when mRNA decay is inhibited.

Summary statement

Pnrc2 promotes decay of tail-shortened, ribosome-disengaged mRNAs and co-regulates *her1* mRNA decay with Ddx6 and Ddx61, P-body factors that sustain normal development in decay-deficient *pnrc2* mutants.

Introduction

In vertebrates, somitogenesis is a fundamental developmental process (Kageyama et al., 2012) characterized by the anterior to posterior sequential segmentation of the embryonic mesoderm into blocks of tissue called somites, which later give rise to axial skeletal muscle, vertebrae, and dermis (Christ et al., 1978; Christ et al, 1986; Keynes and Stern 1988). This rhythmic and regular process is controlled by a molecular oscillator called the segmentation clock which operates in the unsegmented presomitic mesoderm (PSM) and is characterized by rapid cycles of mRNA and protein expression (Hubaud and Pourquie, 2014; Oates et al., 2012; Pourquie, 2011). The segmentation clock is regulated by a self-sustaining negative feedback loop, where a core oscillatory factor, a transcriptional repressor, inhibits expression of downstream oscillatory genes, including itself. In all vertebrates examined to date,

transcriptional repressors of the *Hes*/*her* gene family are considered the conserved pacemakers of the segmentation clock (Bessho et al., 2001; Oates and Ho 2002; Palmeirim et al., 1997).

For proper somite formation, rates of each oscillatory step, from transcription to translation to decay, must be regulated to ensure correct somite size and number (Gomez et al., 2008; Holley et al., 2000; Keynes and Stern 1988; Lewis, 2003; Matsuda et al., 2020; Palmeirim et al., 1997; Schroter and Oates, 2010). Real-time in vivo segmentation clock reporters designed to recapitulate clock dynamics must not only contain critical transcriptional regulatory regions that drive oscillatory expression but must also contain features, typically 3'UTR sequences and protein motifs, that destabilize reporter mRNAs and proteins, respectively (Aulehla et al., 2008; Delaune et al., 2012; Masamizu et al., 2006; Simsek et al., 2023; Yoshioka-Kobayashi et al., 2020).

We have focused on post-transcriptional regulation of the segmentation clock (reviewed in Blatnik et al., 2023) which was originally motivated by our discovery that the zebrafish *pnrc2* gene promotes rapid decay of oscillatory gene transcripts (Dill and Amacher, 2005; Gallagher et al., 2017; Tietz et al., 2020). Pnrc2 (Proline-rich nuclear receptor coactivator 2) is related to the EDC family of mRNA decapping enhancers and contains a large intrinsically disordered domain and domains that facilitate interaction with the Dcp1a mRNA decapping factor and the Upf1 mRNA decay factor (Cho et al., 2009; Lai et al., 2012). Although Pnrc2 has been characterized as a mRNA decay adaptor protein in cell culture, there is no evidence that it directly binds mRNA. Transcriptional oscillations are normal in zebrafish *pnrc2* mutants, but *her1* mRNA (and other oscillatory gene transcripts) accumulate due to mRNA decay defects (Dill and Amacher, 2005; Gallagher et al., 2017; Tietz et al., 2020). Surprisingly, despite a 4-6-fold increase in *her1* and *dlc* oscillatory gene transcripts in *pnrc2* mutants, oscillatory gene protein is expressed normally (Gallagher et al., 2017) and there is no overt segmentation phenotype. Discordance between mRNA and protein levels might be caused by a combination of factors: transcripts might be inefficiently translated due to deadenylation and/or binding of translational repressors, as well as localized to cytoplasmic ribonucleoprotein granules like P-bodies that are sites of non-translating deadenylated mRNAs (reviewed in: Luo et al., 2018; Ostareck et al., 2014). We explore these possibilities using a combination of deep sequencing, molecular, and in vivo approaches.

To better understand the role of *pnrc2* during segmentation, we used RNA-Seq analysis and identified over 1700 transcripts that were significantly overexpressed at least 1.2-fold in *MZpnrc2* mutants. GO analysis reveals enrichment for many biological processes, including terms associated with mRNA processing and decay. Motif analysis shows that overexpressed

transcripts are enriched for well-known RNA binding protein (RBP) and microRNA (miRNA) target sites. Accumulated transcripts of several oscillatory genes have shortened poly(A) tails, suggesting that they are inefficiently translated. Supporting this interpretation, polysome profiling shows that several oscillatory gene transcripts that are overexpressed in *MZpnrc2* mutants have normal levels of ribosome engagement. *MZpnrc2* mutants are sensitive to inhibition of deadenylation and to depletion of the P-body factors Ddx6 and Ddx61, suggesting that accumulated mRNAs in *pnrc2* mutants are not translated when deadenylation and P-body functions are intact. Overall, our results show that discordant expression of oscillatory gene mRNA and protein in *MZpnrc2* mutants is likely due to inefficient translation of accumulated transcripts. In the absence of Pnrc2 function, the P-body factors Ddx6 and Ddx61 buffer against mRNA decay dysfunction and support embryonic development, implicating a broader role for Pnrc2 and P-bodies during development across many tissue types.

Results:

Pnrc2-regulated transcripts are associated with key biological processes and are enriched for destabilizing motifs

During somitogenesis, *pnrc2* promotes decay of oscillatory gene transcripts (Gallagher et al., 2017; Tietz et al., 2020). To globally identify transcripts that require *pnrc2* for proper expression, we performed RNA-Seq analysis on wild-type and maternally-zygotic *pnrc2* (*MZpnrc2*) mutant embryos at mid-segmentation stages. We detected 2,256 significantly differentially expressed transcripts with a false discovery rate of $q < 0.05$ (Fig. 1A, Tables S1-S3) using the program Kallisto to quantify transcript abundance (Bray et al., 2016) and Sleuth for differential expression analysis (Pimentel et al., 2017). Most differentially expressed transcripts were overexpressed (n = 1,769 transcripts), as expected for a mRNA decay-deficient mutant. Among overexpressed transcripts, >99% are annotated as protein-coding by Ensembl's biotype annotation (n = 1759 transcripts), suggesting that Pnrc2 regulates decay of transcripts with full open reading frames rather than transcripts containing premature termination codons that are subject to nonsense-mediated decay (NMD).

To explore characteristics of overexpressed transcripts in *MZpnrc2* mutants, we conducted GO enrichment analysis (Thomas et al., 2022). GO analysis identified many significantly enriched GO terms in the "biological process" aspect (Fig. 1B, Tables S4-S5) including somite specification and neural development, processes that rely upon *Hes/her* oscillations for proper differentiation (Bonev et al., 2012; Hatakeyama et al., 2004; Ishibashi et al., 1995; Ohtsuka et al., 1999; Soto et al., 2020; Tan et al., 2012). Additional enriched terms in

136 the aspects biological process and molecular function are related to developmental pathways
137 involving Fgf, Wnt, Notch, and Ephrin signaling (Figs 1, S1, Table S5). Terms associated with
138 post-transcriptional regulation are also enriched including 3'UTR-mediated destabilization,
139 deadenylation-dependent decay, and P-body assembly (Fig. 1B, Table S5). Overexpressed
140 genes in these categories may represent transcripts that depend on Pnrc2 for their decay or
141 transcripts that are expressed to compensate for loss of Pnrc2 function.
142 Our previous work showed that the Pnrc2-regulated *her1* transcript contains two critical
143 destabilizing motifs in the 3'UTR, a Pumilio Response Element (PRE) and AU-rich Element
144 (ARE) (Tietz et al., 2020). To determine whether 3'UTRs of overexpressed transcripts identified
145 by RNA-Seq analysis of *MZpnrc2* mutants are enriched for PREs, AREs, and additional
146 destabilizing motifs, we performed motif analysis using the MEME Suite tool STREME (Simple,
147 Thorough, Rapid, Enriched Motif Elicitation) that finds motifs in large datasets (Bailey, 2021).
148 Among all 8 statistically significant enriched motifs (Tables S4-S5), the sequences UGUACAU
149 and UGUAAAUA (Fig. 1C) match the destabilizing PRE (Arvola et al., 2020; Bohn et al., 2018;
150 Galgano et al., 2008; Gerber et al., 2006; Hafner et al., 2010; Lu and Hall, 2011; Morris et al.,
151 2008; Murata et al., 1995; Wang et al., 2002; White et al., 2001; Zamore et al., 1997; Zamore et
152 al., 1999). The enriched motifs UAUUUAUU and UAUUAUUA (Fig. 1D) are AREs, motifs that
153 are recognized by a broad group of ARE-binding proteins (ARE-BPs) that can both inhibit and
154 promote mRNA decay and/or translation (Briata et al., 2005; Garneau et al., 2007; Gratacos and
155 Brewer, 2010; Lykke-Andersen and Wagner, 2005; Sanduja et al., 2011). Additional enriched
156 motifs (Fig. 1E) include GUUUGUUU that matches GU-rich elements (GREs), a motif that is
157 associated with mRNA decay (Rattenbacher et al., 2010), and the enriched sequence
158 CCC<u>CCUC</u>C that contains a destabilizing CCUC motif (Vejner et al., 2019). Lastly, we find
159 enrichment for miRNA target sites (Fig. 1F), including the motif K<u>ACUUGA</u> that matches the
160 miR-26 seed target site UACUUGA (Crippa et al., 2016; Icli et al., 2013; Klett et al., 2019;
161 Watterston et al., 2019) and the motif A<u>GCACUU</u> that matches the miR-430 target site
162 GCACUU (Baia Amaral et al., 2024; Bazzini et al., 2012; Giraldez et al., 2006; Liu et al., 2020;
163 Rabani et al., 2017; Vejnar et al., 2019). Enrichment of miRNA target sequences suggests that
164 there is potential cross-talk and/or interactions between Pnrc2- and miRNA-mediated decay.
165 Overall, we find that all significantly enriched 3'UTR motifs are known to destabilize transcripts.
166 Furthermore, STREME analysis of unaffected and under-expressed transcript 3'UTRs (see
167 methods) does not identify enrichment for destabilizing motifs, although unaffected transcript
168 3'UTRs are enriched for AU dinucleotide repeats (Tables S4-S5). Together, these results
169 suggest that Pnrc2 is important for decay of mRNAs with destabilizing 3'UTRs.

170

171 *Loss of Pnrc2 disrupts mRNA expression patterns of many developmental genes*

172 Expression patterns of the oscillatory gene transcripts *her1*, *her7*, and *dlc*, all of which
173 are associated with the GO term somite specification (Fig. 1B), are disrupted in *MZpnrc2*
174 mutants (Gallagher et al., 2017; Tietz et al., 2020). We used in situ hybridization to characterize
175 gene expression patterns and RT-qPCR to validate expression levels of select genes
176 overexpressed by RNA-Seq analysis and associated with segmentation, oscillatory expression,
177 and/or Fgf or Wnt signaling. For in situ hybridization, coloration reactions for each probe were
178 developed in both wild-type and *MZpnrc2* mutant embryos for identical reaction times in parallel.
179 For RT-qPCR, expression levels were quantified using whole embryo extracts from wild-type
180 and *MZpnrc2* mutant embryos at mid-segmentation stages. The expression pattern of *rhov*, an
181 oscillatory gene in zebrafish PSM (Krol et al., 2011), is restricted in wild-type embryos but
182 expanded in *MZpnrc2* mutants (Fig. 2A, A' vs B, B'). Quantification by RT-qPCR validates that
183 *rhov* expression is significantly increased in *MZpnrc2* mutants (Fig. 2C). Expression of *sp5l* (Fig.
184 2D, D' vs E, E', RT-qPCR in F), a gene whose ortholog *Sp5* oscillates in mouse PSM (Krol et al.,
185 2011; Matsuda et al., 2020), is similarly affected. Expression of the somite polarity genes
186 *mespab* and *ripply2 a*lso show expanded expression in *MZpnrc2* mutants (Fig. 2G, G' vs H, H''
187 and J, J' vs K, K', RT-qPCR in I and L). Expression of *dact1*, a modulator of Wnt/b-catenin
188 signaling (Waxman et al., 2004) that oscillates in mouse and human PSM cells (Krol et al., 2011;
189 Matsuda et al., 2020) is also expanded in *MZpnrc2* mutants (Fig. 2M, M' vs N, N', RT-qPCR in
190 O). Expression of *spry1* and *spry4*, genes encoding Fgf signaling antagonists whose orthologs
191 oscillate in mouse and/or human PSM cells (Matsuda et al., 2020) also show expanded
192 expression patterns (Fig. 2P, P' vs Q, Q' and S, S' vs T, T', RT-qPCR in R and U). Additional
193 genes known to oscillate in the zebrafish PSM (Krol et al., 2011) and whose transcripts are
194 overexpressed in *MZpnrc2* mutants were validated by RT-qPCR (Fig. S2). In total, of the 21
195 genes known to oscillate in the zebrafish PSM (Krol et al., 2011), 10 are Pnrc2-regulated.
196 Although 24 oscillatory genes were originally identified in microarray experiments (Krol et al.,
197 2011), annotations for 3 have been removed in GRCz11. Overall, our results show that Pnrc2
198 promotes decay of mRNAs that encode many developmental regulators; however, the lack of
199 overt segmentation or additional developmental phenotypes in *MZpnrc2* mutants suggests that
200 Pnrc2-dependent mRNAs are regulated translationally.

201

202 *Overexpressed oscillatory gene transcripts in MZpnrc2 mutants have shortened poly(A) tails*

203 Despite overexpression of many oscillatory and segmentation-related genes, *MZpnrc2*
204 mutants have no overt segmentation phenotype. Expression of *her1* and *dlc* mRNA is increased
205 4-6 fold in *MZpnrc2* mutants, but the corresponding oscillatory protein is expressed normally,
206 consistent with the lack of segmentation phenotypes (Gallagher et al., 2017; Tietz et al., 2020).
207 Discordance between mRNA and protein levels might be due to deadenylation of accumulated
208 transcripts that leads to inefficient translation. To examine poly(A) (pA) tail length, we performed
209 a G/I-tailing-based pA tail length (PAT) assay and find that although the predominant *her1* pA tail
210 length is ~45 nts in both wild-type and *MZpnrc2* mutant embryos, the length distribution is
211 reduced in *MZpnrc2* mutants, which tend to have shorter tails compared to wild-type embryos
212 (Fig. 3A-B). Because most *her1* transcripts with short pA tails in *MZpnrc2* mutants would likely
213 be transcripts that accumulate due to loss of Pnrc2 function, we quantified *her1* and other
214 oscillatory gene transcripts from extracts derived from pA-enriched and pA-depleted extracts
215 obtained by oligo(dT) bead-based purification (see methods for details). The oscillatory gene
216 transcripts *her1*, *her7*, *dlc*, and *rhov* are all significantly overexpressed in pA-depleted extracts,
217 in contrast to pA-enriched extracts that show no significant differences between wild-type and
218 *MZpnrc2* mutant embryos (Fig. 3C-N). Transcripts with short pA tails may not be efficiently
219 captured using oligo(dT) beads, so we quantified oscillatory gene transcripts using cDNA
220 synthesized from total RNA extracts and primed with oligo(dT) to select for polyadenylated
221 mRNA (rather than priming with random primers as performed for all other quantification
222 experiments). Quantification of oligo(dT)-primed cDNA shows that oscillatory gene transcripts
223 *her1*, *her7*, *dlc*, and *rhov* are all significantly overexpressed in *MZpnrc2* mutants (Fig. S3)
224 indicating that accumulated transcripts, although shortened, are not completely deadenylated.
225 These results are consistent with *her1* PAT assay results showing that *her1* transcripts are not
226 completely deadenylated and instead tend to have short tails in *MZpnrc2* mutants (Fig. 3A-B).
227 Because *MZpnrc2* mutants lack segmentation phenotypes, we hypothesize that accumulated
228 tail-shortened oscillatory gene transcripts are inefficiently translated.
229

230 *Overexpressed P-body associated ddx61 transcripts in MZpnrc2 mutants are substantially*
231 *polyadenylated*

232 Accumulation of mRNA in *MZpnrc2* mutants might lead to localization to cytoplasmic
233 ribonucleoprotein (RNP) granules such as processing bodies (P-bodies) that are sites of
234 translationally repressed transcripts (Luo et al., 2018; Ostareck et al., 2014). In eukaryotic cells,
235 P-body formation is enhanced in cells that accumulate mRNA decay intermediates (Sheth and
236 Parker, 2003; Teixeira et al., 2005) as well as in cells treated with the translational inhibitor

puromycin that results in ribosomes dissociating from mRNAs (Eulalio et al., 2007; Zheng et al., 2008). Transcripts of several genes associated with the enriched GO term “P-body assembly” are overexpressed in *MZpnrc2* mutants (Tables S3 and S5). These include *ddx6* and *ddx61* that are orthologous to the highly conserved *DDX6/p54* DEAD-box helicase gene family that is required for P-body formation (reviewed in: Luo et al., 2018; Ostareck et al., 2014). Of the two zebrafish *ddx6* ohnologs (Singh et al., 2020), *ddx61* expression is more than 16-fold higher than *ddx6* at mid-segmentation stages (White et al., 2017), indicating that *ddx61* is the predominantly expressed ohnolog during segmentation. Upon profiling *ddx61* expression in pA-enriched and pA-depleted extracts, we find that *ddx61* is significantly overexpressed in both fractions (Fig. 3O-Q). Detection of *ddx61* overexpression in pA-enriched extracts suggests that *ddx61* overexpression in *MZpnrc2* mutants might lead to increased Ddx61 protein levels, in contrast to oscillatory gene transcripts for which overexpression is detected only in pA-depleted extracts.

Accumulated oscillatory gene transcripts in MZpnrc2 mutants are disengaged from translational machinery, whereas overexpressed ddx61 transcripts are translationally engaged

Because accumulated oscillatory gene transcripts in *MZpnrc2* mutants have reduced tail lengths, we assessed engagement of *her1* and other oscillatory gene transcripts with ribosomes. We conducted polysome profiling from wild-type and *MZpnrc2* mutant embryos at mid-segmentation stages to compare oscillatory gene transcript levels in actively translating versus non-translating fractions (see methods). The overall polysome profiles are similar in wild-type and *MZpnrc2* mutant embryos (Fig. 4A), suggesting that global translation is normal in mutants; however, *her1* transcripts in *MZpnrc2* mutants are 20-fold higher in unbound/subunit fractions, and not significantly different in monosome- and polysome-bound fractions compared to wild-type *her1* levels (Fig. 4B). Similar distributions were obtained for other oscillatory gene transcripts including *her7*, *dlc*, and *rhov* (Fig. 4C-E). Together, these results support the hypothesis that accumulated oscillatory gene transcripts in *MZpnrc2* mutants are not efficiently translated. Because *ddx61* mRNA is overexpressed in pA-enriched RNA extracts (Fig. 3P), we profiled *ddx61* mRNA abundance across fractions and find that *ddx61* levels are 3-fold higher in *MZpnrc2* polysome fractions relative to wild-type polysome fractions (Fig. 4F). To corroborate polysome profiling results, we performed immunoblot detection of Ddx61 using wild-type and *MZpnrc2* mutant extracts. Ddx6 and Ddx61 cannot be discriminated because both have the same molecular weight and antibodies that distinguish between the two highly similar proteins are not available. Immunoblot results show a corresponding increase in Ddx6/Ddx61 protein levels in *MZpnrc2* mutants at mid-segmentation stages (Fig. 4G-H), corroborating polysome

271 profiling. Overall, our results show that *ddx61* gene products, unlike oscillatory genes, are
272 overexpressed at both mRNA and protein levels in *MZpnrc2* mutants.
273
274 *MZpnrc2 mutants are sensitized to deadenylation inhibition*
275 Because several oscillatory gene transcripts have shortened pA tails in *MZpnrc2*
276 mutants, we hypothesized that blocking deadenylation would alleviate their inefficient translation
277 and lead to segmentation and/or additional phenotypes. Ectopic expression of a CCR4-NOT
278 dominant negative deadenylase via mRNA injection into zebrafish embryos has previously been
279 shown to disrupt segmentation and prevent pA tail shortening of oscillatory gene transcripts
280 including *her1* and *her7* (Fujino et al., 2018). Consistent with the published work, we confirmed
281 that *Myc-Cnot7DN* mRNA injection causes segmentation defects in wild-type embryos, with over
282 84% of injectants exhibiting segmentation defects (Fig. S4). To determine whether *MZpnrc2*
283 mutants are more sensitive to deadenylation inhibition than wild-type embryos, we induced
284 mosaic expression of Myc-tagged Cnot7DN at mid-segmentation stages in embryos injected
285 with a heat shock-inducible construct and scored them for segmentation defects 6 hours post-
286 heat shock (see methods for details). We find that mosaic expression of Myc-Cnot7DN leads to
287 abnormal segment formation in *MZpnrc2* mutants, but not in wild-type embryos (Fig. 5A-E),
288 consistent with the hypothesis that *MZpnrc2* mutants are sensitized to deadenylase inhibition.
289 Using anti-Myc immunohistochemistry on plasmid-injected embryos, we confirmed that *Myc-*
290 *cnot7DN* expression was mosaically induced post-heat shock and was absent in no-heat shock
291 controls (Fig. 5F-G).
292
293 *MZpnrc2 mutants are sensitized to depletion of Ddx61 and Ddx6 function*
294 Because *ddx61* is overexpressed at both mRNA and protein levels, depleting Ddx61
295 function in *MZpnrc2* mutants might lead to segmentation and/or additional phenotypes. Using a
296 highly efficient F0 CRISPR knockdown strategy (Hoshijima et al., 2019; Klatt Shaw and
297 Mokalled, 2021), we find that single *ddx61* crispants (as well as single *ddx6* crispants) develop
298 normally up to 5 days post-fertilization (dpf) and can be raised without significant losses up to
299 adulthood (data not shown). To estimate efficiency of our F0 CRISPR strategy (Fig. S5A), we
300 employed high resolution melt analysis (HRMA) to detect CRISPR-induced mutations and
301 confirmed that all CRISPR-injected embryos were mutagenized (Fig. S5B-C). Because *ddx6*
302 might compensate for loss of *ddx61* function, we also targeted *ddx6*. In *ddx6* and *ddx61* double
303 crispants, *ddx6* and *ddx61* mRNA levels are more than 50% reduced at 18 hpf compared to
304 uninjected sibling controls (Fig. S5D-E), likely because the premature termination codon-

305 containing transcripts created by our targeting strategy are degraded by NMD (reviewed in:
306 Causier et al., 2017; He and Jacobson, 2015; Karousis et al., 2016; Kervestin and Jacobson,
307 2012; Lykke-Andersen and Bennett, 2014; Schoenberg and Maquat, 2012). Corresponding with
308 reduced mRNA levels, Ddx6/Ddx61 protein levels are also reduced in *ddx6*;*ddx61* crispants
309 over time, becoming nearly absent by 5 dpf (Fig. S5F). Coinciding with reduced Ddx6/Ddx61
310 protein levels, we find that *ddx6;ddx61* crispant wild-type and *MZpnrc2* mutant embryos exhibit
311 morphological abnormalities beginning at 2 dpf that worsen with time. By 5 dpf, some
312 *ddx6*;*ddx61* crispant larvae exhibit strong morphological abnormalities, with *MZpnrc2* mutants
313 showing higher frequency and more severe abnormalities than wild-type larvae (Fig. 6A-B).
314 Corresponding with morphological defects, Ddx61/Ddx6 protein is strongly reduced in both
315 *ddx6*;*ddx61* crispant wild-type and *MZpnrc2* mutant embryos at 5 dpf (Figs 6C, S5G-H). The
316 lack of overt phenotypes prior to 2 dpf may be due to maternal contribution that compensates
317 for loss of zygotic function at early stages. Consistent with this possibility, both *ddx61* mRNA
318 and Ddx61 protein are abundant prior to zygotic genome activation according to the Zebrafish
319 Protein Profiling interactive tool (da Silva et al., 2024).
320 Morphological defects in *ddx6;dd61* crispant larvae might be preceded by earlier
321 molecular phenotypes. To determine whether *her1* expression is affected in *ddx6;ddx61*
322 crispants, we performed *her1* in situ hybridization on *ddx6*;*ddx61* crispant wild-type and
323 *MZpnrc2* mutant embryos at mid-segmentation stages. Although the *her1* expression pattern in
324 *ddx6*;*ddx61* crispant wild-type embryos was indistinguishable from uninjected wild-type controls
325 (Fig. 7A,A' vs B,B'), *ddx6*;*ddx61* crispant *MZpnrc2* mutants showed an enhanced misexpression
326 phenotype compared to uninjected *MZpnrc2* mutant controls (Fig. 7C,C' vs D, D'). We
327 separately quantified *her1* levels by RT-qPCR and find that *her1* is increased more than 1.5-fold
328 in *ddx6*;*ddx61* crispant *MZpnrc2* mutants relative to control *MZpnrc2* mutants (Fig. 7E), but is
329 unaffected in *ddx6*;*ddx61* crispant wild-type embryos. In contrast, *her7* expression is modestly
330 reduced, whereas *dlc* and *rhov* expression is unaffected in *ddx6*;*ddx61* crispant *MZpnrc2*
331 mutants (Fig. 7F-H). Overall, normal levels of oscillatory gene transcripts in *ddx6*;*ddx61* crispant
332 wild-type embryos suggest that Ddx61 and Ddx6 are not required for mRNA decay when Pnrc2
333 is functional. The synergistic effect of loss of *pnrc2*, *ddx6*, and *ddx61* shows that Ddx6 and
334 Ddx61 partially compensate for loss of Pnrc2 function.
335

336 **Discussion**

337 In this work, we show that overexpressed transcripts in *MZpnrc2* mutants are enriched
338 for destabilizing sequences. Among overexpressed transcripts, many correspond to genes that

339 are dynamically regulated, including oscillatory and/or developmental genes that function in
340 Notch, Fgf, and Wnt signaling pathways. Remarkably, despite overexpression of >1700
341 transcripts, segmentation and other developmental processes appear normal in *MZpnrc2*
342 mutants, although many fail to thrive as juveniles and adults. We previously suggested that
343 absence of segmentation defects is likely because accumulated mRNAs in *MZpnrc2* mutants
344 are not efficiently translated (Gallagher et al., 2017), though the mechanism was unknown. In
345 the current study, we explored mechanisms driving discordant expression of mRNA and protein
346 in *MZpnrc2* mutants by assessing the polyadenylation status of *her1* and other transcripts, their
347 level of engagement with translational machinery, and the impact of P-body factors Ddx6 and
348 Ddx61 on the *MZpnrc2* overexpression phenotype.
349
350 *Overexpressed transcripts in MZpnrc2 mutants are enriched for destabilizing motifs*
351 Most differentially expressed transcripts in *MZpnrc2* mutants are overexpressed, which
352 we expected based on previous human cell-based studies that showed that PNRC2 functionally
353 interacts with mRNA decay machinery and promotes mRNA decay (Cho et al., 2009; Cho et al.,
354 2012; Cho et al., 2013; Cho et al., 2015; Lai et al., 2012; Mugridge et al., 2016; Nicholson et al.,
355 2018). Motif enrichment analysis of overexpressed transcripts in *MZpnrc2* mutants reveals that
356 PRE and ARE motifs are the most significantly enriched motifs, extending our previous findings
357 that the *her1*, *her7*, and *dlc* 3'UTRs each contain PRE and ARE motifs, and in the case of the
358 *her1* 3'UTR, terminally located PRE and ARE motifs drive rapid decay of reporter mRNA in vivo
359 (Tietz et al., 2020). In eukaryotes, transcriptome-wide profiling has shown that PREs and AREs
360 destabilize mRNA in human and mouse cell lines (Siegel et al., 2022; Schwanhausser et al.,
361 2011; Yang et al., 2003), mouse embryonic stem cells (Sharova et al., 2009), *Drosophila* cell
362 lines (Cairrao et al., 2009) and embryos (Burow et al., 2015), as well as in zebrafish embryos
363 (Rabani et al., 2017; Vejner et al., 2019). Pumilio (Pum) and ARE-binding proteins (ARE-BPs)
364 preferentially bind these motifs, respectively, and recruit deadenylation factors to initiate mRNA
365 decay (Arvola et al., 2020; Bulbrook et al., 2018; Enwerem et al., 2021; Joly et al., 2013;
366 Kadyrova et al., 2007; Weidmann et al., 2014). Because the poly(A) tail promotes translation
367 and mRNA stability, deadenylation leads to reduced translation and enhanced decay (Garneau
368 et al., 2007; Jackson et al., 2010).
369 In zebrafish, a reporter-based study found that PREs and AREs are associated with
370 rapid decay during the maternal-zygotic transition (MZT) (Rabani et al., 2017). Analysis of
371 endogenous transcripts revealed that AREs and CCUC motifs are among the most destabilizing
372 motifs during MZT (Vejner et al., 2019). We found that the C-rich motif CCC<u>CCUC</u>C that

373 contains a CCUC stretch is enriched in overexpressed transcripts in *MZpnrc2* mutants.
374 Similarly, C-rich elements are enriched in 3'UTRs of unstable mRNAs in human induced
375 pluripotent stem cells (Neff et al., 2012). These observations that C-rich sequences are
376 associated with transcript instability are somewhat surprising because C-rich sequences are
377 typically associated with mRNA stability through binding of poly(C)-binding proteins (PCBPs), a
378 family of multifunctional RBPs (Bomsztyk et al., 1997; Makeyev and Liebhaber, 2002; Ostareck-
379 Lederer et al., 1998). The role of C-rich sequences and their associated RBPs is likely context
380 and cell-type dependent, exemplified by the finding that zebrafish Pcbp2 preferentially binds
381 CCUC motifs and is associated with unstable mRNAs during MZT (Vejner et al., 2019). The GU-
382 rich sequence GUUUGUUU is also enriched in the 3'UTRs of overexpressed transcripts; this
383 sequence is found within the known destabilizing GU-rich element (GRE) U<u>GUUUGUUU</u>GU, a
384 3'UTR motif enriched in short-lived mRNAs in primary human T cells and associated with CUG-
385 binding proteins (Halees et al., 2011; Rhagavan et al., 2002; Vlasova et al., 2008).
386 Additional enriched motifs from our analysis include matches to miRNA seed target sites
387 for *miR-26* and *miR-430*. Our previous work showed that *her1* mRNA decay is independent of
388 Dicer-dependent miRNAs (Gallagher et al., 2017), consistent with the absence of either site in
389 the *her1* 3'UTR. Whether other Pnrc2-regulated transcripts utilize miRNA-based regulation for
390 their decay is unknown. miRNAs recruit the two major deadenylation complexes, Pan2-Pan3
391 and CCR4-NOT, to their target mRNAs by association with the miRNA-induced silencing
392 complex (Braun et al., 2011; Chekulaeva et al., 2011; Fabian et al., 2011). However,
393 mechanisms by which miRNAs reduce expression of target mRNAs are context dependent,
394 exemplified by studies using zebrafish embryos during MZT (Bazzini et al., 2012) and studies
395 using *Drosophila* S2 cells (Djuranovic et al., 2012) that showed that miRNA target mRNAs are
396 translationally repressed prior to deadenylation. Destabilizing 3'UTR motifs are associated with
397 translational repression, however distinguishing between direct effects that RBPs and miRNAs
398 bound to target mRNAs have on translational machinery from indirect effects due to
399 deadenylation and decay can be challenging. This is further complicated by the ability of some
400 members of the CCR4-NOT deadenylation complex to recruit translational repressors
401 independent of deadenylation (Cooke et al., 2010; Waghray et al., 2015).
402
403 *Transcripts of many genes that regulate post-transcriptional processes depend on Pnrc2 for*
404 *normal expression levels*
405 Among enriched GO terms identified by analysis of overexpressed transcripts in
406 *MZpnrc2* mutants, some are related to post-transcriptional regulation including "3'UTR-mediated

407 mRNA destabilization, deadenylation-dependent decay" and "P-body assembly". Genes in the
408 first category are primarily *zfp36* family members, with five out of six *zfp36* orthologs
409 overexpressed in *MZpnrc2* mutant embryos (*zfp36l1a*, *zfp36l1l*, *zfp36l2*, *zgc:114130*, and
410 *zgc:162730*). Zfp36 members are CCCH-type zinc finger proteins that bind AREs and
411 destabilize target mRNAs by recruiting deadenylation factors (reviewed in: Blatnik et al., 2023;
412 Ciais et al., 2013; Hau et al., 2007). It is possible that *zfp36* overexpression in *MZpnrc2* mutant
413 embryos leads to an increase in Zfp36 protein levels that enhances deadenylation and reduces
414 excess translation of *pnrc2*-regulated transcripts, however it may simply be that *zfp36*
415 transcripts are *pnrc2*-dependent for their decay. Future analysis of Zfp36 protein levels in
416 *MZpnrc2* mutant embryos coupled with genetic analysis of *zfp36* mutants will provide insight
417 into these possibilities.
418 Enrichment of the GO term "P-body assembly" raises the possibility that mechanisms
419 that sequester mRNAs from translational machinery are active in *MZpnrc2* mutants.
420 Overexpressed transcripts with this GO term include *edc3*, *lsm14aa, ddx6*, and *ddx61.* In yeast,
421 Edc3 is a decapping enhancer that activates decapping and promotes P-body formation
422 (reviewed in: Ditlev et al., 2018; He and Jacobson, 2023). LSm14/RAP55, similarly interacts
423 with decapping factors and promotes P-body formation (reviewed in: Marnef et al., 2009; Vidya
424 and Duchaine, 2022). The conserved Ddx6 family of helicases (also known as Rck/p54) are
425 decapping activators that are required for P-body formation and interact with Edc3, LSm14, and
426 other P-body factors (Luo et al., 2018; Ostareck et al., 2014). Zebrafish possess two Ddx6
427 helicases, Ddx6/P54a and Ddx61/P54b, both of which localize to cytoplasmic granules during
428 zebrafish embryonic development (Zampedri et al., 2016). Among P-body assembly genes, we
429 focused on *ddx6* and *ddx61* because transient knockdown of these genes leads to
430 morphological defects in several tissues including somites (Zampedri et al., 2016) and because
431 DDX6 overexpression in human pluripotent stem cells increases P-body number (Di Stefano et
432 al, 2019). Future analysis of *edc3* and *lsm14aa* will provide further insight into the role of P-
433 bodies during segmentation.
434
435 *Depletion of RNA helicases Ddx6 and Ddx61 leads to developmental defects in MZpnrc2*
436 *mutants*
437 In the current work, we show that Ddx6/Ddx61 RNA helicases are overexpressed at both
438 mRNA and protein levels in *MZpnrc2* mutants. Depletion of *ddx6* and *ddx61* function in *MZpnrc2*
439 mutants, but not wild-type embryos, enhances *her1* accumulation and leads to strong
440 morphological larval phenotypes that are also present at much lower frequency in wild-type

441 crispants. Higher rates of severe larval phenotypes in *ddx6;ddx61 MZpnrc2* crispants compared
442 to wild-type crispants suggest that Pnrc2-regulated transcripts are over-translated upon
443 depletion of Ddx6 and Ddx61 function. It is possible that Ddx6 and Ddx61 promote tail-
444 shortening of accumulated mRNAs in *pnrc2* mutants, similar to what has been shown for human
445 DDX6 that promotes deadenylation of inefficiently translated mRNAs in human cells (Weber and
446 Chang, 2024). We did not observe morphological defects in *ddx6*;*ddx61* crispant embryos at 1
447 dpf in either wild-type or *MZpnrc2* mutant backgrounds, likely due to maternal contribution that
448 compensates for loss of zygotic Ddx6 and Ddx61 function. The absence of an early phenotype
449 differs from previous work which showed that *ddx6* and *ddx61* morpholino (MO) injection leads
450 to somite and notochord defects (Zampedri et al., 2016), which we suspect may be due to MO-
451 induced toxicity and/or off-target effects caused by the high doses used (Schulte-Merker and
452 Stainier, 2014; Stainier et al., 2017). Future work using genetic mutants will help resolve this
453 discrepancy.
454 The finding that *her1* mRNA accumulation in *MZpnrc2* mutants is enhanced in
455 *ddx6*;*ddx61* crispants suggests that P-body factors promote *her1* mRNA decay in the absence
456 of Pnrc2. P-bodies are thought to primarily function as sites of mRNA storage rather than decay,
457 supported by observations that mRNA decay continues even in the absence of P-bodies
458 (Decker et al., 2007; Eulalio et al., 2007; Stoecklin et al., 2006). Early reports of mRNA decay in
459 P-bodies are attributable to artifacts of the MS2 tethering system which inadvertently stabilizes
460 partially degraded reporter mRNAs that subsequently localize in P-bodies (Garcia & Parker,
461 2015; Heinrich et al., 2017; Tutucci et al., 2018). Recent work employing a new tethering
462 method to monitor mRNA dynamics suggests that some mRNAs are degraded rapidly within P-
463 bodies, but decay can be inadvertently inhibited due to stress induced by high laser intensities
464 frequently used during time-lapse imaging (Blake et al., 2024). An alternative explanation for
465 enhanced *her1* accumulation in *ddx6*;*ddx61* crispant *MZpnrc2* mutants is that Ddx6/Ddx61
466 promotes *her1* mRNA decay in a P-body-independent manner, as both RNA helicases show
467 diffuse cytoplasmic expression in addition to enrichment in cytoplasmic foci (Zampedri et al.,
468 2016). A recent human cell culture-based study found that DDX6 binds stalled ribosomes,
469 recruits the CCR4-NOT deadenylase complex, and triggers decay of inefficiently translated
470 mRNAs (Weber and Chang, 2024), an effect that presumably occurs outside of P-bodies. The
471 extent to which *her1* mRNA is degraded in the cytoplasm versus P-bodies as well as the
472 dependence of these activities on Pnrc2 function remains to be explored and future localization
473 studies will shed light on these possibilities.
474

475 **Conclusions**

476 Pnrc2 promotes rapid mRNA decay during vertebrate segmentation, including the decay
477 of many dynamically expressed oscillatory gene transcripts. Overexpressed transcripts in
478 *MZpnrc2* mutants are enriched for destabilizing motifs that are associated with translational
479 repression and mRNA decay. *MZpnrc2* mutant embryos develop normally despite dysfunctional
480 mRNA decay and this is likely because transcripts that depend on Pnrc2 for their rapid decay
481 have shortened poly(A) tails that are inefficiently translated. Consistent with this view, inhibiting
482 deadenylation leads to somite and additional defects in sensitized *MZpnrc2* mutants, likely due
483 to over-translation of Pnrc2-regulated transcripts. Upregulation of *ddx61* at both mRNA and
484 protein levels suggests that compensatory mechanisms are employed in decay-deficient *pnrc2*
485 mutants. The synergistic effect of loss of *pnrc2*, *ddx6*, and *ddx61* leads to strong developmental
486 phenotypes, suggesting that accumulated mRNAs are translated in *pnrc2* mutants upon
487 depletion of the RNA helicases Ddx6 and Ddx61. Overall, our results show that Ddx6 and
488 Ddx61 regulate *her1* oscillatory expression and likely ensure proper protein levels in mRNA-
489 decay deficient mutants.
490

491 **Materials and methods**

492 **Animal stocks and husbandry**

493 All protocols using zebrafish were approved by the Ohio State University Institutional Animal
494 Care and Use Committee (protocol 2012A00000113-R4). Adult zebrafish strains (*Danio rerio*)
495 were kept at 28.5°C on a 14 hour (h) light/10 h dark cycle and obtained by natural spawning or
496 *in vitro* fertilization (Westerfield, 2007). Embryos and larvae were staged according to Kimmel et
497 al.,1995. The *pnrc2*^{oz22} line has been described previously (Gallagher et al., 2017).
498

499 **DNA extraction and genotyping**

500 Individual embryos and adult fin tissue were lysed in 50 ul 1X ThermoPol Buffer (NEB) at 95°C
501 for 10 minutes, digested at 55°C for 1 hour in 1 mg/ml Proteinase K (BP1700, ThermoFisher),
502 followed by Proteinase K inactivation at 95°C for 10 minutes. Molecular identification of *pnrc2*^{oz22}
503 carriers by PCR amplification followed by NsiI-HF digestion to distinguish cleavable wild-type
504 from uncleavable mutant amplicons was performed as previously described (Tietz et al., 2020).
505

506 **RNA-Seq sample collection and sequencing**

507 Whole embryos at mid-segmentation stages (n = 50 embryos per biological replicate for each
508 genotype) were solubilized in Trizol for RNA extraction and purified following standard

509 procedures (Thermo Fisher). Both wild-type and *MZpnrc2* mutant embryo samples were
510 prepared in biological triplicate. 2 ug of total RNA from each sample was processed at
511 Novogene using a whole transcriptome sequencing workflow with ribosomal RNA (rRNA)
512 depletion that enables sequencing of RNA irrespective of polyadenylation status. At Novogene,
513 each sample was depleted of rRNA using a Ribo-Zero Kit (Illumina), followed by chemical
514 fragmentation and 150 bp paired-end library synthesis using a NEBNext Ultra II Directional RNA
515 kit (NEB). Libraries were sequenced on the Illumina NovaSeq 6000 platform by Novogene.
516
517 **RNA-Seq data analysis**
518 High-throughput sequencing reads were trimmed to remove adapter and primer sequences
519 using Cutadapt version 3.4 (Martin, 2011) and pseudoaligned to the zebrafish
520 GRCz11/danRer11 transcriptome reference using Kallisto (version 0.46.2), an RNA-Seq tool
521 that rapidly quantifies transcript abundance without the need for individual base alignment (Bray
522 et al., 2016). Cutadapt and Kallisto were installed and run in Python (version 2.7.5) using
523 standard procedures described in online guides available at
524 https://cutadapt.readthedocs.io/en/stable/guide.html and
525 https://pachterlab.github.io/kallisto/manual. Prior to running Kallisto, all sequence data files were
526 assessed using the quality control tool FastQC version 0.12.1 (Andrews, 2010) and no quality
527 issues were identified in relevant modules for RNA-Seq analysis (data not shown). Transcripts
528 with <5 estimated read counts in at least one sample were filtered out to reduce noise.
529 Differential gene expression analysis was performed using Sleuth version 0.30.1, a program
530 that uses variance decomposition to identify biological differences between RNA-Seq samples
531 (Pimentel et al., 2017). Sleuth was run in RStudio version 2023.06.2 Build 561 (Posit Software)
532 using standard procedures described in an online guide at
533 https://pachterlab.github.io/sleuth_walkthroughs/trapnell/analysis.html. Batch effects including
534 effects due to sequencing lane or biological replicate differences were tested and no effects
535 were observed (data not shown). A summary of the RNA-Seq processed data, Kallisto
536 normalized read counts, and Sleuth-generated differential expression results are included as
537 supplementary data (Tables S1-S3).
538
539 **Motif analysis**
540 Motif analysis was performed using 3'UTR input sequences corresponding to transcripts
541 identified from RNA-Seq analysis of *MZpnrc2* mutant embryos (Tables S3-S4) and the MEME
542 Suite tool STREME version 5.5.6 (Bailey et al., 2021). Annotated 3'UTR sequences from each

543 of the following datasets were analyzed using STREME: 1) significantly overexpressed
544 transcripts (q < 0.05; n = 1320), 2) unaffected transcripts (log2FC from -0.05 to 0.05; n = 1334),
545 and 3) significantly under-expressed transcripts (i.e. transcripts with decreased expression in
546 *MZpnrc2* mutants relative to wild-type embryos; q < 0.05; n = 690) (Tables S3-S4). 3'UTR
547 sequence annotations were obtained using BioMart (Ensembl release 113, GRCz11 assembly)
548 and those less than 50 nts in length were removed to reduce annotation and length biases.
549 Motif range was set to 6-8 nts and shuffled input sequences were used as the control with
550 Markov order set to 2 (the default setting used by STREME). Sequence logos (Schneider and
551 Stephens, 1990; Schneider et al., 1986) were generated using probability matrix data from
552 STREME and the seqLogo package (Bembom and Ivanek, 2024) available with BioConductor
553 version 3.19 (Gentleman et al., 2004; Huber et al., 2015) in RStudio version 2023.06.2 Build
554 561 (Posit Software). Motif enrichment results are reported in Table S5.
555

556 **GO analysis**

557 GO analysis was performed using the PANTHER Overrepresentation Test (Released 2024-02-
558 26) that is available from the Gene Ontology Consortium at https://geneontology.org/ (Mi et al.,
559 2013; Thomas et al., 2022). The GO Ontology database version used was DOI:
560 10.5281/zenodo.10536401 (Released 2024-01-17). The input list contains gene IDs for which at
561 least one transcript was significantly overexpressed (q < 0.05) in *MZpnrc2* mutants and for
562 which a GO annotation was identified (n = 1619 uniquely annotated GO IDs) (Table S4), while
563 the reference list contains the full set of GO-annotated zebrafish genes in the database (n =
564 26,353). GO results are reported in Table S5. Statistical test type was a Fisher's Exact test
565 corrected by calculating the false discovery rate.
566

567 **In situ hybridization**

568 Whole mount in situ hybridization was performed as previously described (Broadbent and Read,
569 1999; Jowett, 1998) using digoxygenin (DIG)-labeled riboprobes. Riboprobe for *her1* was
570 previously described (Delaune et al., 2012; Dill and Amacher, 2005). Riboprobe for *rhov* was
571 synthesized from a plasmid containing the *rhov* cDNA (cb832) received from the Zebrafish
572 International Resource Center (ZIRC). *rhov*-containing plasmid was linearized with NotI-HF
573 (NEB) and transcribed with T7 RNA polymerase (Roche Life Science) to make DIG-labeled
574 antisense *rhov* riboprobe. Riboprobe templates for *sp5l*, *mespab*, *ripply2*, *dact1*, *spry1*, and
575 *spry4* were generated by PCR amplification of coding sequence (primer sequences are listed in
576 Table S6). All DIG-labeled PCR-based probes were synthesized by transcribing PCR templates

with SP6 or T7 RNA polymerase (Roche Life Science). *dact1*, *sp5l*, and *spry4* produced expression patterns consistent with direct submission in situ hybridization data (Thisse et al., 2001; Thisse et al., 2005). Additionally, expression patterns for all PCR-based probes shown in Fig. 2 match published expression patterns for wild-type embryos at mid-segmentation stages, including *dact1* (Gillhouse et al., 2004), *mespab* (Cutty et al., 2012; Wanglar et al., 2014), *sp5l* (Superina et al., 2014), *ripply2* (Junker et al., 2014; Kinoshita et al., 2018; Moreno et al., 2008; Wanglar et al., 2014; Yabe et al., 2016), *spry1* (Komisarczuk et al., 2008), and *spry4* (Nguyen-Chi et al., 2012). In situ hybridized embryos were mounted in Permount and imaged using an Axiocam HRc digital camera with AxioPlan2 microscope and 10x objective (Zeiss).

RNA extraction and cDNA synthesis

Whole embryos at mid-segmentation stages (n = 15 embryos per biological replicate for each genotype in Fig. 2; n = 10 embryos per biological replicate for each genotype and condition in Fig. 7) were solubilized in Trizol for RNA extraction and purified following standard procedures (Thermo Fisher). All genotypes and conditions were performed in biological triplicate. 500 ng of total RNA was reverse transcribed with random primers and Superscript IV reverse transcriptase according to the manufacturer's instructions (Thermo Fisher).

Quantitative RT-PCR analysis

Quantitative RT-PCR was performed using PowerUp SYBR Green Master Mix (Thermo Fisher) and 4.5 ul cDNA (diluted 1:50 in Fig. 2, diluted 1:25 in Fig. 7) in 20 ul reactions, following manufacturer's procedures. Negative controls lacking template were included for each primer set. All reactions were subjected to thermal melting to confirm that each reaction gave single peaks. Transcript levels were normalized to *mobk13* (*mob4*) (Gangras et al., 2020; Hu et al., 2016; Tietz et al., 2020). Cycle thresholds (Ct) were determined using CFX Maestro version 2.3 software (Bio-Rad). The average Ct of 2-3 technical replicates per sample was used for calculations. Changes in mRNA expression were calculated by $\Delta\Delta Ct = \Delta Ct$ target $- \Delta Ct$ control. Relative changes in mRNA expression levels are represented graphically as fold change, where relative mRNA fold change = $2^{-\Delta\Delta Ct}$. All graphs and statistics were generated using Prism 10 (GraphPad).

Poly(A) Tail-Length Assay

RNA for poly(A) tail-length assays was obtained by collecting whole embryos at mid-segmentation stages (n = 18 embryos for each genotype) followed by solubilization in Trizol and

611 purification following standard manufacturer procedures (Thermo Fisher). Tail-lengths for *her1*
612 transcripts were assessed using the Poly(A) Tail-Length Assay Kit following standard
613 manufacturer procedures (Thermo Fisher). Minus RT controls were performed for all samples
614 and no amplification was detected as expected (data not shown). Primers used for tail-length
615 assay PCR are listed in Table S6.
616
617 **Preparation and analysis of poly(A)-enriched and poly(A)-depleted extracts**
618 RNA for comparison of expression levels in poly(A)-enriched versus poly(A)-depleted RNA
619 fractions was obtained from the same RNA sources as was used for RNA-Seq experiments
620 described earlier. Three biological replicates were obtained for both wild-type and *MZpnrc2*
621 mutant embryos. From each sample, 1 ug of total RNA was adjusted to a final volume of 50 ul in
622 bead binding buffer (20 mM Tri-HCl, pH 7.5, 1.0 M LiCl, and 2 mM EDTA) and incubated with
623 Dynabeads Oligo$(dT)_{25}$ following manufacturer procedures (Thermo Fisher). RNA bound to
624 beads (poly(A)-enriched RNA) was eluted in 10 mM Tris-HCl (pH 7.5). Unbound RNA (poly(A)-
625 depleted RNA) was precipitated by adding 0.1x volume 3M sodium acetate and 2x volume ice-
626 cold ethanol, followed by vortexing and incubation overnight at -80°C. After centrifugation at 4°C
627 for 20 minutes at 12,000 x g, precipitated pellets from unbound RNA fractions were rinsed with
628 ice-cold 70% ethanol and resuspended in 10 mM Tris-HCl (pH 7.5) at an equivalent volume
629 used for elution of bound RNA fractions. Each RNA fraction was reverse transcribed using
630 random primers and Superscript IV reverse transcriptase (RT) according to the manufacturer's
631 instructions (Thermo Fisher). As a control, 1 ug of total RNA from the same samples used for
632 bead-based fractionation were reverse transcribed in parallel. RT-qPCR analysis was performed
633 as described earlier using 4.5 ul of cDNA diluted 1:10.
634
635 **Protein extraction and Immunoblot analysis**
636 Protein extracts were prepared from zebrafish embryos or larvae at 1-5 days post-fertilization.
637 Individuals were collected and washed twice with rapid pipetting to disrupt yolks in 200 ul of ice-
638 cold Ringer's solution with protease inhibitors (116 mM NaCl, 2.9 mM KCl, 5.0 mM HEPES, pH
639 7.2, 100 mg/mL Soybean Trypsin Inhibitor [Sigma], 0.2 mg/mL PMSF, Complete Protease
640 Inhibitor Cocktail [Roche]). Embryo and larval suspensions were centrifuged at 4°C for 1 minute
641 at 300 x g for each wash. Cell lysis was performed by addition of 1 ul 4X LDS Buffer (Thermo
642 Fisher) for each embryo or larva collected (n = 20-65 individuals per extraction), followed by
643 homogenization with a plastic pestle, vortexing for 1 minute, and boiling for 10 minutes.
644 Homogenization, vortexing, and boiling were performed twice sequentially. Embryo or larval

645 equivalents were loaded on a 4-12% Novex Bis-Tris polyacrylamide gel (Thermo Fisher),
646 electrophoresed in NuPAGE MOPS SDS running buffer (Thermo Fisher) alongside a Novex
647 Sharp pre-stained protein standard (Thermo Fisher), and transferred to a PVDF membrane
648 using the Bio-Rad wet transfer system following standard manufacturer procedures. Immunoblot
649 was blocked in 5% non-fat skim milk in Tris-buffered saline (20 mM Tris, 150 mM NaCl, pH 7.5)
650 and subsequent steps were performed following standard procedures available online from Bio-
651 Rad in bulletin 6376 (https://www.bio-rad.com/). The immunoblot was incubated with DDX6
652 antibody (A16270, AbClonal) followed by incubation with AP-conjugated goat anti-rabbit IgG
653 (H+L) secondary antibody (Thermo Fisher). Immunoblots were then incubated with β-actin (sc-
654 47778, Santa Cruz Biotechnology) antibody followed by incubation with AP-conjugated goat
655 anti-mouse IgG (H+L) secondary antibody (Thermo Fisher). Primaries were diluted 1:1000 and
656 secondaries were diluted 1:10,000 in blocking solution with 0.1% Tween-20. Primary antibody
657 incubations were performed overnight at 4°C, secondary antibody incubations were performed
658 for 1 hour at room temperature. Chemiluminescent detection was performed using CDP-Star
659 following the manufacturer's procedure (Thermo Fisher) and imaged using the Sapphire FL
660 Biomolecular Imager (Azure Biosystems). Quantification of signal intensities was performed
661 using lane profile analysis in Alpha Imager software (Protein Simple).
662

663 **Plasmid construction & transgenesis**

664 The heat shock construct *hsp70l:Myc-cnot7DN-SV40 pA* was assembled by first constructing
665 plasmid *pMA-Myc-cnot7DN* using the GeneArt Plasmid Construction Service (Thermo Fisher).
666 *pMA-Myc-cnot7DN* contains the coding sequence for a dominant negative form of zebrafish
667 *Cnot7* (*Cnot7DN*) with an N-terminal C-myc epitope tag (Evan et al., 1985) and intervening
668 SGLRS flexible linker peptide. The *myc*-tagged *Cnot7DN* coding sequence was based on
669 plasmid M338 (*pCS2* + *MT-CNOT7-D40A,E42E,C67E,L71E-sv40*) that has previously been
670 used to inhibit deadenylase function in zebrafish embryos (Fujino et al., 2018; Makino et al.,
671 2015; Mishima and Tomari, 2016; Mishima and Tomari, 2017). After sequence validation of
672 *pMA-Myc-cnot7DN*, the *Myc-cnot7DN* insert was cloned into *pBSKI2* (Thermes et al., 2002)
673 using standard restriction digestion-based cloning with the enzymes NheI-HF and BamHI-HF
674 (NEB). Plasmid and I-SceI enzyme were injected into the blastomere of 1-cell stage wild-type
675 and *MZpnrc2* mutant embryos following standard transgenesis procedures (Thermes et al.,
676 2002). To determine the optimal dose, we injected 20 pg and 60 pg plasmid doses in the
677 absence of heat-shock induction and assessed morphology at mid-segmentation stages; the 20

678 pg dose was well-tolerated (73 of 90 injected embryos had wild-type morphology), but the 60 pg
679 dose caused gross abnormalities (0 of 56 injected embryos had wild-type morphology).
680
681 **Heat shock assay**
682 Plasmid-injected embryos (described above) were collected and raised to segmentation stages
683 (10-12S), heat shocked at 37°C for 30 minutes, and monitored for somite defects at 30 minute
684 intervals post-heat shock (pHS). Live embryos at 6 hours post-heat shock were mounted in 3%
685 methylcellulose and imaged at 20x magnification using AxioVision Software (Zeiss) on a
686 MZFLIII Fluorescence Stereo Microscope (Leica) with an AxioCam HRc digital camera (Zeiss)
687 and subsequently fixed in 4% PFA for anti-Myc immunohistochemistry.
688
689 **Anti-Myc Immunohistochemistry**
690 Embryos injected with *hsp70l:Myc-cnot7DN* plasmid that were heat shocked at ~14 hours post
691 fertilization (hpf) for 30 minutes were collected 6 hours post-heat shock (~22 hpf) alongside non-
692 heat shocked controls, fixed in 4% PFA in PBS overnight at 4°C, and washed 5 x 5 minutes in
693 PBS with 0.1% Tween-20 (PBST). Embryos were then incubated in water for 5 minutes,
694 permeabilized with ice-cold acetone for 7 minutes, and incubated again in water for 5 minutes
695 followed by 3 x 5 minute PBST washes. Blocking was performed in PBST with 2% BSA, 2%
696 goat serum for 1 hour at room temperature, followed by incubation with 1:500 dilution
697 monoclonal anti-myc (clone 9E10, MA1-980, Thermo Fisher) in PBS with 2% BSA, 2% goat
698 serum, 1% DMSO and 0.1% Triton X-100 (PBDTx) overnight at 4°C. Embryos were washed 8 x
699 15 minutes in PBST, blocked as described above, followed by incubation with 1:200 dilution
700 Alexa Fluor 546 goat anti-mouse secondary antibody (Thermo Fisher) in PBDTx overnight at
701 4°C. Embryos were washed 8 x 15 minutes in PBST prior to imaging. Immuno-stained embryos
702 were mounted in Fluoromount-G and imaged at 20x magnification using AxioVision Software
703 (Zeiss) on an MZFLIII Fluorescence Stereo Microscope (Leica) with a mCherry filter set and
704 AxioCam HRc digital camera (Zeiss).
705
706 **Polysome profiling**
707 Wild-type and *MZpnrc2* mutant embryos were raised to mid-segmentation stages and treated in
708 100 ug/ml cycloheximide for 5 minutes (n = 300 embryos per biological replicate for each
709 genotype). Embryos were triturated using a 200 ul pipette and washed to remove yolks as
710 previously described (Link et al., 2006) except that E2 embryo medium containing
711 cycloheximide (15 mM NaCl, 0.7 mM $NaHCO_3$, 0.5 mM KCl, 0.15 mM KH_2PO_4, 2.7 mM $CaCl_2$,

712 0.5 mM Na_2HPO_4, 1mM $MgSO_4$, 100 ug/ml cycloheximide) was used in lieu of 0.5x Ginzburg
713 Fish Ringer's buffer. Cell pellets were resuspended in 500 ul of chilled lysis buffer (20 mM Tris
714 HCl pH 7.5, 30 mM $MgCl_2$, 100 mM NaCl, 0.5 uM DTT, 100 ug/ml cycloheximide, 1 mg/ml
715 heparin, 2.5 ul/ml NP-40) and incubated on ice for 10 minutes. Lysates were centrifuged at
716 12,000 x g for 10 minutes at 4°C to fractionate nuclei and debris (pellet) from cytoplasm
717 (supernatant). After total RNA quantification of cytoplasmic extracts on a Nanodrop
718 Spectrophotometer (Thermo Fisher), a volume corresponding to 50 ug of total RNA was
719 transferred onto a 10-50% linear sucrose density gradient per sample. Gradients were
720 centrifuged at 35,000 x g for 2-3 hours at 4°C. Following centrifugation, gradients were
721 fractionated into 12, 1 ml fractions using a BioComp Piston Gradient Fractionator and A_{260nm}
722 profiles were recorded using a BioComp Triax Flow Cell.
723
724 **RNA extraction of polysome fractions**
725 From each fraction, 400 ul was used for the following procedure. To each fraction, 2 ng
726 *Luciferase* Control RNA (Promega) was added as a normalization spike-in control, followed by
727 600 ul of Trizol and purification following standard procedures (Thermo Fisher). RNA pellets
728 were rinsed with ice-cold 70% ethanol, briefly dried, and resuspended in 20 ul nuclease-free
729 H_2O. For each fraction, 8 ul of RNA was reverse transcribed using random primers and
730 Superscript IV reverse transcriptase following the manufacturer's instructions (Thermo Fisher).
731
732 **CRISPR-Cas9 mutagenesis of *ddx6* and *ddx61***
733 CRISPR RNA (crRNA) guide sequences were designed using Integrated DNA Technologies
734 (IDT) custom design tool
735 (https://www.idtdna.com/site/order/designtool/index/CRISPR_CUSTOM). crRNA sequences with
736 the highest on-target scores with no predicted off-target sites were chosen. The impact of
737 targeted mutations on gene function was maximized by targeting regions within exons encoding
738 the DEAD box helicase domain (see Fig. S5A-B). Reagents for CRISPR-Cas9 mutagenesis
739 were prepared as previously described for efficient mutagenesis (Shaw & Mokalled, 2001).
740 Briefly, crRNAs targeting *ddx6* and *ddx61* (25 uM each, 50 uM total) and trans-activating
741 CRISPR RNA (tracrRNA) (IDT) (50 uM) were combined equally and annealed to generate dual
742 guide RNA duplexes (dgRNA), followed by 1:1 dilution in duplex buffer (IDT) for a final
743 concentration of 25 uM dgRNA. Annealed dgRNAs were next combined equally with 25 uM
744 Cas9-NLS (QB3 MacroLab, UC Berkeley) that had been diluted from a 40 uM stock solution
745 using Cas9 dilution buffer B (IDT). Final injection solutions contained 0.1% phenol red dye, 0.2

M potassium chloride, and 5 uM each of dgRNA and Cas9-NLS. Injection solutions were incubated for 5 minutes at 37°C to facilitate ribonucleoprotein complex (RNP) formation. AB wild-type embryos were injected at the 1-cell stage with 2 nl of injection solution. crRNA sequences are listed in Table S6.

Acknowledgements

We thank the Ohio State Zebrafish Facilities staff for excellent zebrafish care, the Ohio Supercomputer Center for computational resources, the Genomics Shared Resource at the Ohio State Comprehensive Cancer Center for RNA quality analysis and DNA sequencing, and the Ohio State Center for RNA Biology for their support and resources. We thank Susan Cole, Kenneth Poss, Mira Pronobis, and Guramrit Singh for advice and critical comments. We also thank Anton Blatnik, Geremy Lerma, Ryan Denniston, Lauren Levesque, Benjamin Pastore, and Zhongxia Yi for advice.

Competing interests

The authors declare no competing or financial interests.

Funding

This work was supported by NIH grants R01GM117964 (to S.L.A.) and R35GM146924 (to M.G.K.), an OSU Dean's Enrichment Fellowship (to M.C.B.), a Pelotonia Fellowship (to M.C.B.), an OSU Center for RNA Biology Undergraduate Fellowship (to K.G.T.), and a Cellular, Molecular, and Biochemical Sciences T32 Training fellowship T32GM141955 (to C.C.A.).

Data and resource availability

RNA-Seq datasets will be made available with repository name and identifier at publication. All additional data and details of resources can be found within the article and its supplementary information.

Author contributions

T.L.G., M.C.B., C.C.A, K.G.T, D.M.P, A.M., and S.L.A. performed experiments. T.L.G., M.C.B., M.G.K., and S.L.A. analyzed data. All authors contributed intellectually and discussed the data and manuscript. T.L.G. wrote the manuscript and all authors participated in the editing process.

References

Andrews, S. (2010). FastQC - A quality control tool for high throughput sequence data. http://www.bioinformatics.babraham.ac.uk/projects/fastqc/. *Babraham Bioinformatics*.

Aulehla, A., Wiegraebe, W., Baubet, V., Wahl, M. B., Deng, C., Taketo, M., Lewandoski, M. and Pourquié, O. (2008). A beta-catenin gradient links the clock and wavefront systems in mouse embryo segmentation. *Nat Cell Biol* **10**, 186–193.

Baia Amaral, D., Egidy, R., Perera, A. and Bazzini, A. A. (2024). miR-430 regulates zygotic mRNA during zebrafish embryogenesis. *Genome Biol* **25**, 74.

Bailey, T. L. (2021). STREME: accurate and versatile sequence motif discovery. *Bioinformatics* **37**, 2834–2840.

Bazzini, A. A., Lee, M. T. and Giraldez, A. J. (2012). Ribosome profiling shows that miR-430 reduces translation before causing mRNA decay in zebrafish. *Science* **336**, 233–237.

Bembom, O. and Ivanek, R. (2024). seqLogo: Sequence logos for DNA sequence alignments.

Benjamini, Y., Krieger, A. M. and Yekutieli, D. (2006). Adaptive linear step-up procedures that control the false discovery rate. *Biometrika* **93**, 491–507.

Bessho, Y., Sakata, R., Komatsu, S., Shiota, K., Yamada, S. and Kageyama, R. (2001). Dynamic expression and essential functions of Hes7 in somite segmentation. *Genes Dev* **15**, 2642–2647.

Blake, L. A., Watkins, L., Liu, Y., Inoue, T. and Wu, B. (2024). A Rapid Inducible RNA Decay system reveals fast mRNA decay in P-bodies. *Nat Commun* **15**, 2720.

Blatnik, M. C., Gallagher, T. L. and Amacher, S. L. (2023). Keeping development on time: Insights into post-transcriptional mechanisms driving oscillatory gene expression during vertebrate segmentation. *Wiley Interdiscip Rev RNA* **14**, e1751–e1751.

Bohn, J. A., Van Etten, J. L., Schagat, T. L., Bowman, B. M., McEachin, R. C., Freddolino, L. and Goldstrohm, A. C. (2018). Identification of diverse target RNAs that are functionally regulated by human Pumilio proteins. *Nucleic Acids Res* **46**, 362–386.

Bomsztyk, K., Van Seuningen, I., Suzuki, H., Denisenko, O. and Ostrowski, J. (1997). Diverse molecular interactions of the hnRNP K protein. *FEBS Lett* **403**, 113–115.

Bonev, B., Stanley, P. and Papalopulu, N. (2012). MicroRNA-9 Modulates Hes1 ultradian oscillations by forming a double-negative feedback loop. *Cell Rep* **2**, 10–18.

Bonferroni, C. E. (1935). Il Calcolo delle Assicurazioni su Gruppi di Teste. In *Studi in Onore del Professore Salvatore Ortu Carboni*.

Bonferroni, C. E. (1936). Teoria statistica delle classi e calcolo delle probabilità. *Pubblicazioni del R Istituto Superiore di Scienze Economiche e Commerciali di Firenze* **8**, 3–62.

Braun, J. E., Huntzinger, E., Fauser, M. and Izaurralde, E. (2011). GW182 Proteins Directly Recruit Cytoplasmic Deadenylase Complexes to miRNA Targets. *Mol Cell* **44**, 120–133.

Bray, N. L., Pimentel, H., Melsted, P. and Pachter, L. (2016). Near-optimal probabilistic RNA-seq quantification. *Nat Biotechnol* **34**, 525–527.

Briata, P., Forcales, S. V., Ponassi, M., Corte, G., Chen, C.-Y., Karin, M., Puri, P. L. and Gherzi, R. (2005). p38-Dependent Phosphorylation of the mRNA Decay-Promoting Factor KSRP Controls the Stability of Select Myogenic Transcripts. *Mol Cell* **20**, 891–903.

Bulbrook, D., Brazier, H., Mahajan, P., Kliszczak, M., Fedorov, O., Marchese, F. P., Aubareda, A., Chalk, R., Picaud, S., Strain-Damerell, C., et al. (2018). Tryptophan-Mediated Interactions between Tristetraprolin and the CNOT9 Subunit Are Required for CCR4-NOT Deadenylase Complex Recruitment. *J Mol Biol* **430**, 722–736.

Burow, D. A., Umeh-Garcia, M. C., True, M. B., Bakhaj, C. D., Ardell, D. H. and Cleary, M. D. (2015). Dynamic regulation of mRNA decay during neural development. *Neural Dev* **10**, 11.

Cairrao, F., Halees, A. S., Khabar, K. S. A., Morello, D. and Vanzo, N. (2009). AU-rich elements regulate Drosophila gene expression. *Mol Cell Biol* **29**, 2636–2643.

Causier, B., Li, Z., De Smet, R., Lloyd, J. P. B., Van de Peer, Y. and Davies, B. (2017). Conservation of Nonsense-Mediated mRNA Decay Complex Components Throughout Eukaryotic Evolution. *Sci Rep* **7**, 16692.

Chekulaeva, M., Mathys, H., Zipprich, J. T., Attig, J., Colic, M., Parker, R. and Filipowicz, W. (2011). miRNA repression involves GW182-mediated recruitment of CCR4-NOT through conserved W-containing motifs. *Nat Struct Mol Biol* **18**, 1218–1226.

Cho, H., Kim, K. M. and Kim, Y. K. (2009). Human Proline-Rich Nuclear Receptor Coregulatory Protein 2 Mediates an Interaction between mRNA Surveillance Machinery and Decapping Complex. *Mol Cell* **33**, 75–86.

Cho, H., Kim, K. M., Han, S., Choe, J., Park, S. G., Choi, S. S. and Kim, Y. K. (2012). Staufen1-Mediated mRNA Decay Functions in Adipogenesis. *Mol Cell* **46**, 495–506.

Cho, H., Han, S., Choe, J., Park, S. G., Choi, S. S. and Kim, Y. K. (2013). SMG5-PNRC2 is functionally dominant compared with SMG5-SMG7 in mammalian nonsense-mediated mRNA decay. *Nucleic Acids Res* **41**, 1319–1328.

Cho, H., Park, O. H., Park, J., Ryu, I., Kim, J., Ko, J. and Kim, Y. K. (2015). Glucocorticoid receptor interacts with PNRC2 in a ligand-dependent manner to recruit UPF1 for rapid mRNA degradation. *Proc Natl Acad Sci U S A* **112**, E1540–E1549.

845 **Christ, B., Jacob, H. J. and Jacob, M.** (1978). On the formation of the myotomes in avian
846 embryos. An experimental and scanning electron microscope study. *Experientia* **34**, 514–
847 516.
848 **Christ, B., Jacob, M., Jacob, H.J., Brand, B., Wachtler, F.** (1986). Myogenesis: A Problem of
849 Cell Distribution and Cell Interactions. In: Bellairs, R., Ede, D.A., Lash, J.W. (eds) Somites in
850 Developing Embryos. NATO ASI Series, vol 118. Springer, Boston, MA.
851 **Ciais, D., Cherradi, N. and Feige, J.-J.** (2013). Multiple functions of tristetraprolin/TIS11 RNA-
852 binding proteins in the regulation of mRNA biogenesis and degradation. *Cell Mol Life Sci* **70**,
853 2031–2044.
854 **Cooke, A., Prigge, A. and Wickens, M.** (2010). Translational repression by deadenylases. *J*
855 *Biol Chem* **285**, 28506–28513.
856 **Crippa, S., Nemir, M., Ounzain, S., Ibberson, M., Berthonneche, C., Sarre, A., Boisset, G.,**
857 **Maison, D., Harshman, K., Xenarios, I., Diviani, D., Schorderet D., Pedrazzini, T.** (2016).
858 Comparative transcriptome profiling of the injured zebrafish and mouse hearts identifies
859 miRNA-dependent repair pathways. *Cardiovasc Res* **110**, 73–84.
860 **Cutty, S. J., Fior, R., Henriques, P. M., Saúde, L. and Wardle, F. C.** (2012). Identification and
861 expression analysis of two novel members of the Mesp family in zebrafish. *Int J Dev Biol* **56**,
862 285–294.
863 **da Silva Pescador, G., Baia Amaral, D., Varberg, J. M., Zhang, Y., Hao, Y., Florens, L. and**
864 **Bazzini, A. A.** (2024). Protein profiling of zebrafish embryos unmasks regulatory layers
865 during early embryogenesis. *Cell Rep* **43**, 114769.
866 **Decker, C. J., Teixeira, D. and Parker, R.** (2007). Edc3p and a glutamine/asparagine-rich
867 domain of Lsm4p function in processing body assembly in Saccharomyces cerevisiae. *J Cell*
868 *Biol* **179**, 437–449.
869 **Delaune, E. A., François, P., Shih, N. P. and Amacher, S. L.** (2012). Single-cell-resolution
870 imaging of the impact of Notch signaling and mitosis on segmentation clock dynamics. *Dev*
871 *Cell* **23**, 995–1005.
872 **Dill, K. K. and Amacher, S. L.** (2005). tortuga refines Notch pathway gene expression in the
873 zebrafish presomitic mesoderm at the post-transcriptional level. *Dev Biol* **287**, 225–236.
874 **Di Stefano, B., Luo, E.-C., Haggerty, C., Aigner, S., Charlton, J., Brumbaugh, J., Ji, F.,**
875 **Rabano Jiménez, I., Clowers, K. J., Huebner, A. J., et al.** (2019). The RNA Helicase
876 DDX6 Controls Cellular Plasticity by Modulating P-Body Homeostasis. *Cell Stem Cell* **25**,
877 622-638.e13.

Ditlev, J. A., Case, L. B. and Rosen, M. K. (2018). Who's In and Who's Out-Compositional Control of Biomolecular Condensates. *J Mol Biol* **430**, 4666–4684.

Djuranovic, S., Nahvi, A. and Green, R. (2012). miRNA-mediated gene silencing by translational repression followed by mRNA deadenylation and decay. *Science* **336**, 237–240.

Dunn, O. J. (1961). Multiple Comparisons among Means. *J Am Stat Assoc* **56**, 52–64.

Enwerem, I. I. I., Elrod, N. D., Chang, C.-T., Lin, A., Ji, P., Bohn, J. A., Levdansky, Y., Wagner, E. J., Valkov, E. and Goldstrohm, A. C. (2021). Human Pumilio proteins directly bind the CCR4-NOT deadenylase complex to regulate the transcriptome. *RNA* **27**, 445–464.

Eulalio, A., Behm-Ansmant, I., Schweizer, D. and Izaurralde, E. (2007). P-body formation is a consequence, not the cause, of RNA-mediated gene silencing. *Mol Cell Biol* **27**, 3970–3981.

Fujino, Y., Yamada, K., Sugaya, C., Ooka, Y., Ovara, H., Ban, H., Akama, K., Otosaka, S., Kinoshita, H., Yamasu, K., et al. (2018). Deadenylation by the CCR4-NOT complex contributes to the turnover of *hairy*-related mRNAs in the zebrafish segmentation clock. *FEBS Lett* **592**, 3388–3398.

Galgano, A., Forrer, M., Jaskiewicz, L., Kanitz, A., Zavolan, M. and Gerber, A. P. (2008). Comparative analysis of mRNA targets for human PUF-family proteins suggests extensive interaction with the miRNA regulatory system. *PLoS One* **3**, e3164–e3164.

Gallagher, T. L., Tietz, K. T., Morrow, Z. T., McCammon, J. M., Goldrich, M. L., Derr, N. L. and Amacher, S. L. (2017). Pnrc2 regulates 3'UTR-mediated decay of segmentation clock-associated transcripts during zebrafish segmentation. *Dev Biol* **429**, 225–239.

Gangras, P., Gallagher, T. L., Parthun, M. A., Yi, Z., Patton, R. D., Tietz, K. T., Deans, N. C., Bundschuh, R., Amacher, S. L. and Singh, G. (2020). Zebrafish rbm8a and magoh mutants reveal EJC developmental functions and new 3'UTR intron-containing NMD targets. *PLoS Genet* **16**, e1008830–e1008830.

Garcia, J. F. and Parker, R. (2015). MS2 coat proteins bound to yeast mRNAs block 5' to 3' degradation and trap mRNA decay products: implications for the localization of mRNAs by MS2-MCP system. *RNA* **21**, 1393–1395.

Garneau, N. L., Wilusz, J. and Wilusz, C. J. (2007). The highways and byways of mRNA decay. *Nat Rev Mol Cell Biol* **8**, 113–126.

Gentleman, R. C., Carey, V. J., Bates, D. M., Bolstad, B., Dettling, M., Dudoit, S., Ellis, B., Gautier, L., Ge, Y., Gentry, J., et al. (2004). Bioconductor: open software development for computational biology and bioinformatics. *Genome Biol* **5**, R80–R80.

Gerber, A. P., Luschnig, S., Krasnow, M. A., Brown, P. O. and Herschlag, D. (2006). Genome-wide identification of mRNAs associated with the translational regulator PUMILIO in Drosophila melanogaster. *Proc Natl Acad Sci U S A* **103**, 4487–4492.

Gillhouse, M., Wagner Nyholm, M., Hikasa, H., Sokol, S. Y. and Grinblat, Y. (2004). Two *Frodo/Dapper* homologs are expressed in the developing brain and mesoderm of zebrafish. *Developmental Dynamics* **230**, 403–409.

Giraldez, A. J., Cinalli, R. M., Glasner, M. E., Enright, A. J., Thomson, J. M., Baskerville, S., Hammond, S. M., Bartel, D. P. and Schier, A. F. (2005). MicroRNAs Regulate Brain Morphogenesis in Zebrafish. *Science (1979)* **308**, 833–838.

Giraldez, A. J., Mishima, Y., Rihel, J., Grocock, R. J., Van Dongen, S., Inoue, K., Enright, A. J. and Schier, A. F. (2006). Zebrafish MiR-430 Promotes Deadenylation and Clearance of Maternal mRNAs. *Science (1979)* **312**, 75–79.

Gomez, C., Özbudak, E. M., Wunderlich, J., Baumann, D., Lewis, J. and Pourquié, O. (2008). Control of segment number in vertebrate embryos. *Nature* **454**, 335–339.

Gratacós, F. M. and Brewer, G. (2010). The role of AUF1 in regulated mRNA decay. *Wiley Interdiscip Rev RNA* **1**, 457–473.

Hafner, M., Landthaler, M., Burger, L., Khorshid, M., Hausser, J., Berninger, P., Rothballer, A., Ascano Jr, M., Jungkamp, A.-C., Munschauer, M., et al. (2010). Transcriptome-wide identification of RNA-binding protein and microRNA target sites by PAR-CLIP. *Cell* **141**, 129–141.

Halees, A. S., Hitti, E., Al-Saif, M., Mahmoud, L., Vlasova-St Louis, I. A., Beisang, D. J., Bohjanen, P. R. and Khabar, K. (2011). Global assessment of GU-rich regulatory content and function in the human transcriptome. *RNA Biol* **8**, 681–691.

Hatakeyama, J., Bessho, Y., Katoh, K., Ookawara, S., Fujioka, M., Guillemot, F. and Kageyama, R. (2004). *Hes*genes regulate size, shape and histogenesis of the nervous system by control of the timing of neural stem cell differentiation. *Development* **131**, 5539–5550.

Hau, H. H., Walsh, R. J., Ogilvie, R. L., Williams, D. A., Reilly, C. S. and Bohjanen, P. R. (2006). Tristetraprolin recruits functional mRNA decay complexes to ARE sequences. *J Cell Biochem* **100**, 1477–1492.

He, F. and Jacobson, A. (2015). Nonsense-Mediated mRNA Decay: Degradation of Defective Transcripts Is Only Part of the Story. *Annu Rev Genet* **49**, 339–366.

He, F. and Jacobson, A. (2023). Eukaryotic mRNA decapping factors: molecular mechanisms and activity. *FEBS J* **290**, 5057–5085.

Heinrich, S., Sidler, C. L., Azzalin, C. M. and Weis, K. (2017). Stem-loop RNA labeling can affect nuclear and cytoplasmic mRNA processing. *RNA* **23**, 134–141.

Holley, S. A., Geisler, R. and Nüsslein-Volhard, C. (2000). Control of *her1* expression during zebrafish somitogenesis by a *Delta*-dependent oscillator and an independent wave-front activity. *Genes Dev* **14**, 1678–1690.

Hoshijima, K., Jurynec, M. J., Klatt Shaw, D., Jacobi, A. M., Behlke, M. A. and Grunwald, D. J. (2019). Highly Efficient CRISPR-Cas9-Based Methods for Generating Deletion Mutations and F0 Embryos that Lack Gene Function in Zebrafish. *Dev Cell* **51**, 645-657.e4.

Hu, Y., Xie, S. and Yao, J. (2016). Identification of Novel Reference Genes Suitable for qRT-PCR Normalization with Respect to the Zebrafish Developmental Stage. *PLoS One* **11**, e0149277–e0149277.

Hubaud, A. and Pourquié, O. (2014). Signalling dynamics in vertebrate segmentation. *Nat Rev Mol Cell Biol* **15**, 709–721.

Huber, W., Carey, V. J., Gentleman, R., Anders, S., Carlson, M., Carvalho, B. S., Bravo, H. C., Davis, S., Gatto, L., Girke, T., et al. (2015). Orchestrating high-throughput genomic analysis with Bioconductor. *Nat Methods* **12**, 115–121.

Icli, B., Wara, A. K. M., Moslehi, J., Sun, X., Plovie, E., Cahill, M., Marchini, J. F., Schissler, A., Padera, R. F., Shi, J., Cheng, H., Raghuram, S., Arany, Z., Liao, R., Croce, K., MacRae, C., Feinberg, M. (2013). MicroRNA-26a regulates pathological and physiological angiogenesis by targeting BMP/SMAD1 signaling. *Circ Res* **113**, 1231–1241.

Icli, B., Dorbala, P. and Feinberg, M. W. (2014). An emerging role for the miR-26 family in cardiovascular disease. *Trends Cardiovasc Med* **24**, 241–248.

Ishibashi, M., Ang, S. L., Shiota, K., Nakanishi, S., Kageyama, R. and Guillemot, F. (1995). Targeted disruption of mammalian hairy and Enhancer of split homolog-1 (HES-1) leads to up-regulation of neural helix-loop-helix factors, premature neurogenesis, and severe neural tube defects. *Genes Dev* **9**, 3136–3148.

Jackson, R. J., Hellen, C. U. T. and Pestova, T. V (2010). The mechanism of eukaryotic translation initiation and principles of its regulation. *Nat Rev Mol Cell Biol* **11**, 113–127.

Joly, W., Chartier, A., Rojas-Rios, P., Busseau, I. and Simonelig, M. (2013). The CCR4 deadenylase acts with Nanos and Pumilio in the fine-tuning of Mei-P26 expression to promote germline stem cell self-renewal. *Stem Cell Reports* **1**, 411–424.

Junker, J. P., Noël, E. S., Guryev, V., Peterson, K. A., Shah, G., Huisken, J., McMahon, A. P., Berezikov, E., Bakkers, J. and van Oudenaarden, A. (2014). Genome-wide RNA Tomography in the Zebrafish Embryo. *Cell* **159**, 662–675.

Kadyrova, L. Y., Habara, Y., Lee, T. H. and Wharton, R. P. (2007). Translational control of maternal *Cyclin B* mRNA by Nanos in the *Drosophila* germline. *Development* **134**, 1519–1527.

Karousis, E. D., Nasif, S. and Mühlemann, O. (2016). Nonsense-mediated mRNA decay: novel mechanistic insights and biological impact. *Wiley Interdiscip Rev RNA* **7**, 661–682.

Kervestin, S. and Jacobson, A. (2012). NMD: a multifaceted response to premature translational termination. *Nat Rev Mol Cell Biol* **13**, 700–712.

Keynes, R. J. and Stern, C. D. (1988). Mechanisms of vertebrate segmentation. *Development* **103**, 413–429.

Kimmel, C. B., Ballard, W. W., Kimmel, S. R., Ullmann, B. and Schilling, T. F. (1995). Stages of embryonic development of the zebrafish. *Developmental Dynamics* **203**, 253–310.

Klatt Shaw, D. and Mokalled, M. H. (2021). Efficient CRISPR/Cas9 mutagenesis for neurobehavioral screening in adult zebrafish. *G3 (Bethesda)* **11**, jkab089.

Klett, H., Jürgensen, L., Most, P., Busch, M., Günther, F., Dobreva, G., Leuschner, F., Hassel, D., Busch, H. and Boerries, M. (2018). Delineating the Dynamic Transcriptome Response of mRNA and microRNA during Zebrafish Heart Regeneration. *Biomolecules* **9**, 11.

Komisarczuk, A. Z., Topp, S., Stigloher, C., Kapsimali, M., Bally-Cuif, L. and Becker, T. S. (2008). Enhancer detection and developmental expression of zebrafish *sprouty1*, a member of the *fgf8* synexpression group. *Developmental Dynamics* **237**, 2594–2603.

Krol, A. J., Roellig, D., Dequéant, M.-L., Tassy, O., Glynn, E., Hattem, G., Mushegian, A., Oates, A. C. and Pourquié, O. (2011). Evolutionary plasticity of segmentation clock networks. *Development* **138**, 2783–2792.

Kusov, Y. Y., Shatirishvili, G., Dzagurov, G. and Gauss-Müller, V. (2001). A new G-tailing method for the determination of the poly(A) tail length applied to hepatitis A virus RNA. *Nucleic Acids Res* **29**, E57-e57.

Lai, T., Cho, H., Liu, Z., Bowler, M. W., Piao, S., Parker, R., Kim, Y. K. and Song, H. (2012). Structural Basis of the PNRC2-Mediated Link between mRNA Surveillance and Decapping. *Structure* **20**, 2025–2037.

Lewis, J. (2003). Autoinhibition with Transcriptional Delay. *Current Biology* **13**, 1398–1408.

Liu, Y., Zhu, Z., Ho, I. H. T., Shi, Y., Li, J., Wang, X., Chan, M. T. V and Cheng, C. H. K. (2020). Genetic Deletion of miR-430 Disrupts Maternal-Zygotic Transition and Embryonic Body Plan. *Front Genet* **11**, 853.

1012 **Lu, G. and Hall, T. M. T.** (2011). Alternate modes of cognate RNA recognition by human
1013 PUMILIO proteins. *Structure* **19**, 361–367.
1014 **Luo, Y., Na, Z. and Slavoff, S. A.** (2018). P-Bodies: Composition, Properties, and Functions.
1015 *Biochemistry* **57**, 2424–2431.
1016 **Lykke-Andersen, J. and Bennett, E. J.** (2014). Protecting the proteome: Eukaryotic
1017 cotranslational quality control pathways. *J Cell Biol* **204**, 467–476.
1018 **Lykke-Andersen, J. and Wagner, E.** (2005). Recruitment and activation of mRNA decay
1019 enzymes by two ARE-mediated decay activation domains in the proteins TTP and BRF-1.
1020 *Genes Dev* **19**, 351–361.
1021 **Makeyev, A. V and Liebhaber, S. A.** (2002). The poly(C)-binding proteins: a multiplicity of
1022 functions and a search for mechanisms. *RNA* **8**, 265–278.
1023 **Makino, S., Mishima, Y., Inoue, K. and Inada, T.** (2015). Roles of mRNA fate modulators Dhh1
1024 and Pat1 in TNRC6-dependent gene silencing recapitulated in yeast. *J Biol Chem* **290**,
1025 8331–8347.
1026 **Marnef, A., Sommerville, J. and Ladomery, M. R.** (2009). RAP55: Insights into an
1027 evolutionarily conserved protein family. *The International Journal of Biochemistry & Cell*
1028 *Biology* **41**, 977–981.
1029 **Martin, M.** (2011). Cutadapt removes adapter sequences from high-throughput sequencing
1030 reads. *EMBnet J* **17**, 10.
1031 **Martin, G. and Keller, W.** (1998). Tailing and 3'-end labeling of RNA with yeast poly(A)
1032 polymerase and various nucleotides. *RNA* **4**, 226-230.
1033 **Masamizu, Y., Ohtsuka, T., Takashima, Y., Nagahara, H., Takenaka, Y., Yoshikawa, K.,**
1034 **Okamura, H. and Kageyama, R.** (2006). Real-time imaging of the somite segmentation
1035 clock: revelation of unstable oscillators in the individual presomitic mesoderm cells. *Proc*
1036 *Natl Acad Sci U S A* **103**, 1313–1318.
1037 **Matsuda, M., Hayashi, H., Garcia-Ojalvo, J., Yoshioka-Kobayashi, K., Kageyama, R.,**
1038 **Yamanaka, Y., Ikeya, M., Toguchida, J., Alev, C. and Ebisuya, M.** (2020). Species-specific
1039 segmentation clock periods are due to differential biochemical reaction speeds. *Science*
1040 *(1979)* **369**, 1450–1455.
1041 **Mi, H., Muruganujan, A. and Thomas, P. D.** (2013). PANTHER in 2013: modeling the evolution
1042 of gene function, and other gene attributes, in the context of phylogenetic trees. *Nucleic*
1043 *Acids Res* **41**, D377–D386.
1044 **Mishima, Y. and Tomari, Y.** (2016). Codon Usage and 3′ UTR Length Determine Maternal
1045 mRNA Stability in Zebrafish. *Mol Cell* **61**, 874–885.

1046 **Mishima, Y. and Tomari, Y.** (2017). Pervasive yet nonuniform contributions of Dcp2 and Cnot7
1047 to maternal mRNA clearance in zebrafish. *Genes to Cells* **22**, 670–678.
1048 **Moreno, T. A., Jappelli, R., Izpisúa Belmonte, J. C. and Kintner, C.** (2008). Retinoic acid
1049 regulation of the Mesp-Ripply feedback loop during vertebrate segmental patterning. *Dev*
1050 *Biol* **315**, 317–330.
1051 **Morris, A. R., Mukherjee, N. and Keene, J. D.** (2008). Ribonomic analysis of human Pum1
1052 reveals cis-trans conservation across species despite evolution of diverse mRNA target sets.
1053 *Mol Cell Biol* **28**, 4093–4103.
1054 **Mugridge, J. S., Ziemniak, M., Jemielity, J. and Gross, J. D.** (2016). Structural basis of
1055 mRNA-cap recognition by Dcp1-Dcp2. *Nat Struct Mol Biol* **23**, 987–994.
1056 **Murata, Y. and Wharton, R. P.** (1995). Binding of pumilio to maternal hunchback mRNA is
1057 required for posterior patterning in drosophila embryos. *Cell* **80**, 747–756.
1058 **Neff, A. T., Lee, J. Y., Wilusz, J., Tian, B. and Wilusz, C. J.** (2012). Global analysis reveals
1059 multiple pathways for unique regulation of mRNA decay in induced pluripotent stem cells.
1060 *Genome Res* **22**, 1457–1467.
1061 **Nguyen-Chi, M. E., Bryson-Richardson, R., Sonntag, C., Hall, T. E., Gibson, A., Sztal, T.,**
1062 **Chua, W., Schilling, T. F. and Currie, P. D.** (2012). Morphogenesis and cell fate
1063 determination within the adaxial cell equivalence group of the zebrafish myotome. *PLoS*
1064 *Genet* **8**, e1003014–e1003014.
1065 **Nicholson, P., Gkratsou, A., Josi, C., Colombo, M. and Mühlemann, O.** (2018). Dissecting
1066 the functions of SMG5, SMG7, and PNRC2 in nonsense-mediated mRNA decay of human
1067 cells. *RNA* **24**, 557–573.
1068 **Oates, A. C. and Ho, R. K.** (2002). *Hairy/E(spl)-related*(*Her*) genes are central components of
1069 the segmentation oscillator and display redundancy with the Delta/Notch signaling pathway
1070 in the formation of anterior segmental boundaries in the zebrafish. *Development* **129**, 2929–
1071 2946.
1072 **Oates, A. C., Morelli, L. G. and Ares, S.** (2012). Patterning embryos with oscillations: structure,
1073 function and dynamics of the vertebrate segmentation clock. *Development* **139**, 625–639.
1074 **Ohtsuka, T., Ishibashi, M., Gradwohl, G., Nakanishi, S., Guillemot, F. and Kageyama, R.**
1075 (1999). Hes1 and Hes5 as notch effectors in mammalian neuronal differentiation. *EMBO J*
1076 **18**, 2196–2207.
1077 **Ostareck, D. H., Naarmann-de Vries, I. S. and Ostareck-Lederer, A.** (2014). DDX6 and its
1078 orthologs as modulators of cellular and viral RNA expression. *WIREs RNA* **5**, 659–678.

1079 **Ostareck-lederer, A., Ostareck, D. H. and Hentze, M. W.** (1998). Cytoplasmic regulatory
1080 functions of the KH-domain proteins hnRNPs K and E1/E2. *Trends Biochem Sci* **23**, 409–
1081 411.
1082 **Palmeirim, I., Henrique, D., Ish-Horowicz, D. and Pourquié, O.** (1997). Avian hairy Gene
1083 Expression Identifies a Molecular Clock Linked to Vertebrate Segmentation and
1084 Somitogenesis. *Cell* **91**, 639–648.
1085 **Pimentel, H., Bray, N. L., Puente, S., Melsted, P. and Pachter, L.** (2017). Differential analysis
1086 of RNA-seq incorporating quantification uncertainty. *Nat Methods* **14**, 687–690.
1087 **Pourquié, O.** (2011). Vertebrate segmentation: from cyclic gene networks to scoliosis. *Cell* **145**,
1088 650–663.
1089 **Presnyak, V. and Coller, J.** (2013). The DHH1/RCKp54 family of helicases: an ancient family of
1090 proteins that promote translational silencing. *Biochim Biophys Acta* **1829**, 817–823.
1091 **Rabani, M., Pieper, L., Chew, G.-L. and Schier, A. F.** (2017). A Massively Parallel Reporter
1092 Assay of 3' UTR Sequences Identifies In Vivo Rules for mRNA Degradation. *Mol Cell* **68**,
1093 1083-1094.e5.
1094 **Raghavan, A., Ogilvie, R. L., Reilly, C., Abelson, M. L., Raghavan, S., Vasdewani, J.,**
1095 **Krathwohl, M. and Bohjanen, P. R.** (2002). Genome-wide analysis of mRNA decay in
1096 resting and activated primary human T lymphocytes. *Nucleic Acids Res* **30**, 5529–5538.
1097 **Rattenbacher, B., Beisang, D., Wiesner, D. L., Jeschke, J. C., von Hohenberg, M., St**
1098 **Louis-Vlasova, I. A. and Bohjanen, P. R.** (2010). Analysis of CUGBP1 targets identifies
1099 GU-repeat sequences that mediate rapid mRNA decay. *Mol Cell Biol* **30**, 3970–3980.
1100 **Salkind, N.** (2007). *Encyclopedia of Measurement and Statistics*. Sage Publications, Inc.
1101 **Sanduja, S., Blanco, F. F. and Dixon, D. A.** (2011). The roles of TTP and BRF proteins in
1102 regulated mRNA decay. *Wiley Interdiscip Rev RNA* **2**, 42–57.
1103 **Schneider, T. D. and Stephens, R. M.** (1990). Sequence logos: a new way to display
1104 consensus sequences. *Nucleic Acids Res* **18**, 6097–6100.
1105 **Schneider, T. D., Stormo, G. D., Gold, L. and Ehrenfeucht, A.** (1986). Information content of
1106 binding sites on nucleotide sequences. *J Mol Biol* **188**, 415–431.
1107 **Schoenberg, D. R. and Maquat, L. E.** (2012). Regulation of cytoplasmic mRNA decay. *Nat Rev*
1108 *Genet* **13**, 246–259.
1109 **Schröter, C. and Oates, A. C.** (2010). Segment Number and Axial Identity in a Segmentation
1110 Clock Period Mutant. *Current Biology* **20**, 1254–1258.

1111 **Schulte-Merker, S. and Stainier, D. Y. R.** (2014). Out with the old, in with the new: reassessing
1112 morpholino knockdowns in light of genome editing technology. *Development* **141**, 3103–
1113 3104.
1114 **Schwanhäusser, B., Busse, D., Li, N., Dittmar, G., Schuchhardt, J., Wolf, J., Chen, W. and**
1115 **Selbach, M.** (2011). Global quantification of mammalian gene expression control. *Nature*
1116 **473**, 337–342.
1117 **Sharova, L. V, Sharov, A. A., Nedorezov, T., Piao, Y., Shaik, N. and Ko, M. S. H.** (2009).
1118 Database for mRNA half-life of 19 977 genes obtained by DNA microarray analysis of
1119 pluripotent and differentiating mouse embryonic stem cells. *DNA Res* **16**, 45–58.
1120 **Sheth, U. and Parker, R.** (2003). Decapping and decay of messenger RNA occur in
1121 cytoplasmic processing bodies. *Science* **300**, 805–808.
1122 **Sidák, Z.** (1967). Rectangular Confidence Regions for the Means of Multivariate Normal
1123 Distributions. *J Am Stat Assoc* **62**, 626–633.
1124 **Siegel, D. A., Le Tonqueze, O., Biton, A., Zaitlen, N. and Erle, D. J.** (2022). Massively parallel
1125 analysis of human 3' UTRs reveals that AU-rich element length and registration predict
1126 mRNA destabilization. *G3 (Bethesda)* **12**, jkab404.
1127 **Simsek, M. F., Chandel, A. S., Saparov, D., Zinani, O. Q. H., Clason, N. and Özbudak, E. M.**
1128 (2023). Periodic inhibition of Erk activity drives sequential somite segmentation. *Nature* **613**,
1129 153–159.
1130 **Singh, P. P. and Isambert, H.** (2020). OHNOLOGS v2: a comprehensive resource for the
1131 genes retained from whole genome duplication in vertebrates. *Nucleic Acids Res* **48**, D724–
1132 D730.
1133 **Soto, X., Biga, V., Kursawe, J., Lea, R., Doostdar, P., Thomas, R. and Papalopulu, N.**
1134 (2020). Dynamic properties of noise and Her6 levels are optimized by miR-9, allowing the
1135 decoding of the Her6 oscillator. *EMBO J* **39**, e103558–e103558.
1136 **Stainier, D. Y. R., Raz, E., Lawson, N. D., Ekker, S. C., Burdine, R. D., Eisen, J. S., Ingham,**
1137 **P. W., Schulte-Merker, S., Yelon, D., Weinstein, B. M., et al.** (2017). Guidelines for
1138 morpholino use in zebrafish. *PLoS Genet* **13**, e1007000–e1007000.
1139 **Stoecklin, G., Mayo, T. and Anderson, P.** (2006). ARE-mRNA degradation requires the 5'-3'
1140 decay pathway. *EMBO Rep* **7**, 72–77.
1141 **Superina, S., Borovina, A. and Ciruna, B.** (2014). Analysis of maternal-zygotic ugdh mutants
1142 reveals divergent roles for HSPGs in vertebrate embryogenesis and provides new insight
1143 into the initiation of left–right asymmetry. *Dev Biol* **387**, 154–166.

1144 **Tan, S., Ohtsuka, T., González, A. and Kageyama, R.** (2012). MicroRNA9 regulates neural
1145 stem cell differentiation by controlling Hes1 expression dynamics in the developing brain.
1146 *Genes to Cells* **17**, 952–961.
1147 **Teixeira, D., Sheth, U., Valencia-Sanchez, M. A., Brengues, M. and Parker, R.** (2005).
1148 Processing bodies require RNA for assembly and contain nontranslating mRNAs. *RNA* **11**,
1149 371–382.
1150 **Thermes, V., Grabher, C., Ristoratore, F., Bourrat, F., Choulika, A., Wittbrodt, J. and Joly,**
1151 **J.-S.** (2002). I-SceI meganuclease mediates highly efficient transgenesis in fish. *Mech Dev*
1152 **118**, 91–98.
1153 **Thisse, B. and Thisse, C.** (2005). High Throughput Expression Analysis of ZF-Models
1154 Consortium Clones. *ZFIN Direct Data Submission (http://zfin.org)*.
1155 **Thisse, B., Pflumio, S., Furthauer, M., Loppin, B., Heyer, V., Degrave, A., Woehl, R., Lux,**
1156 **A., Steffan, T., Charbonnier, X. Q., et al.** (2001). Expression of the zebrafish genome
1157 during embryogenesis. *ZFIN Direct Data Submission (http://zfin.org)*.
1158 **Thomas, P. D., Ebert, D., Muruganujan, A., Mushayahama, T., Albou, L.-P. and Mi, H.**
1159 (2022). PANTHER: Making genome-scale phylogenetics accessible to all. *Protein Sci* **31**, 8–
1160 22.
1161 **Tietz, K. T., Gallagher, T. L., Mannings, M. C., Morrow, Z. T., Derr, N. L. and Amacher, S. L.**
1162 (2020). Pumilio response and AU-rich elements drive rapid decay of Pnrc2-regulated cyclic
1163 gene transcripts. *Dev Biol* **462**, 129–140.
1164 **Tutucci, E., Vera, M., Biswas, J., Garcia, J., Parker, R. and Singer, R. H.** (2018). An improved
1165 MS2 system for accurate reporting of the mRNA life cycle. *Nat Methods* **15**, 81–89.
1166 **Vejnar, C. E., Abdel Messih, M., Takacs, C. M., Yartseva, V., Oikonomou, P., Christiano, R.,**
1167 **Stoeckius, M., Lau, S., Lee, M. T., Beaudoin, J.-D., et al.** (2019). Genome wide analysis of
1168 3' UTR sequence elements and proteins regulating mRNA stability during maternal-to-
1169 zygotic transition in zebrafish. *Genome Res* **29**, 1100–1114.
1170 **Vidya, E. and Duchaine, T. F.** (2022). Eukaryotic mRNA Decapping Activation. *Front Genet* **13**,
1171 832547.
1172 **Vlasova, I. A., Tahoe, N. M., Fan, D., Larsson, O., Rattenbacher, B., Sternjohn, J. R.,**
1173 **Vasdewani, J., Karypis, G., Reilly, C. S., Bitterman, P. B., et al.** (2008). Conserved GU-
1174 rich elements mediate mRNA decay by binding to CUG-binding protein 1. *Mol Cell* **29**, 263–
1175 270.
1176 **Waghray, S., Williams, C., Coon, J. J. and Wickens, M.** (2015). Xenopus CAF1 requires
1177 NOT1-mediated interaction with 4E-T to repress translation in vivo. *RNA* **21**, 1335–1345.

1178 **Wang, X., McLachlan, J., Zamore, P. D. and Hall, T. M. T.** (2002). Modular Recognition of RNA
1179 by a Human Pumilio-Homology Domain. *Cell* **110**, 501–512.
1180 **Wanglar, C., Takahashi, J., Yabe, T. and Takada, S.** (2014). Tbx protein level critical for clock-
1181 mediated somite positioning is regulated through interaction between Tbx and Ripply. *PLoS*
1182 *One* **9**, e107928–e107928.
1183 **Watterston, C., Zeng, L., Onabadejo, A. and Childs, S. J.** (2019). MicroRNA26 attenuates
1184 vascular smooth muscle maturation via endothelial BMP signalling. *PLoS Genet* **15**,
1185 e1008163–e1008163.
1186 **Waxman, J. S.** (2005). Regulation of the early expression patterns of the zebrafish Dishevelled-
1187 interacting proteins Dapper1 and Dapper2. *Developmental Dynamics* **233**, 194–200.
1188 **Weber, R. and Chang, C.-T.** (2024). Human DDX6 regulates translation and decay of
1189 inefficiently translated mRNAs. *Elife* **13**,.
1190 **Weidmann, C. A., Raynard, N. A., Blewett, N. H., Van Etten, J. and Goldstrohm, A. C.**
1191 (2014). The RNA binding domain of Pumilio antagonizes poly-adenosine binding protein and
1192 accelerates deadenylation. *RNA* **20**, 1298–1319.
1193 **Westerfield, M.** (2007). The Zebrafish Book. A Guide for the Laboratory Use of Zebrafish (Danio
1194 rerio), 5th Edition. *University of Oregon Press, Eugene (Book)*.
1195 **White, E. K., Moore-Jarrett, T. and Ruley, H. E.** (2001). PUM2, a novel murine Puf protein,
1196 and its consensus RNA-binding site. *RNA* **7**, 1855-1866.
1197 **White, R. J., Collins, J. E., Sealy, I. M., Wali, N., Dooley, C. M., Digby, Z., Stemple, D. L.,**
1198 **Murphy, D. N., Billis, K., Hourlier, T., et al.** (2017). A high-resolution mRNA expression
1199 time course of embryonic development in zebrafish. *Elife* **6**, e30860.
1200 **Yabe, T., Hoshijima, K., Yamamoto, T. and Takada, S.** (2016). Quadruple zebrafish mutant
1201 reveals different roles of Mesp genes in somite segmentation between mouse and zebrafish.
1202 *Development* **143**, 2842–2852.
1203 **Yang, E., van Nimwegen, E., Zavolan, M., Rajewsky, N., Schroeder, M., Magnasco, M. and**
1204 **Darnell Jr, J. E.** (2003). Decay rates of human mRNAs: correlation with functional
1205 characteristics and sequence attributes. *Genome Res* **13**, 1863–1872.
1206 **Yoshioka-Kobayashi, K., Matsumiya, M., Niino, Y., Isomura, A., Kori, H., Miyawaki, A. and**
1207 **Kageyama, R.** (2020). Coupling delay controls synchronized oscillation in the segmentation
1208 clock. *Nature* **580**, 119–123.
1209 **Zamore, P. D., Williamson, J. R. and Lehmann, R.** (1997). The Pumilio protein binds RNA
1210 through a conserved domain that defines a new class of RNA-binding proteins. *RNA* **3**,
1211 1421-1433.

1212 **Zamore, P. D., Bartel, D. P., Lehmann, R. and Williamson, J. R.** (1998). The PUMILIO−RNA
1213 Interaction: A Single RNA-Binding Domain Monomer Recognizes a Bipartite Target
1214 Sequence. *Biochemistry* **38**, 596–604.
1215 **Zampedri, C., Tinoco-Cuellar, M., Carrillo-Rosas, S., Diaz-Tellez, A., Ramos-Balderas, J.**
1216 **L., Pelegri, F. and Maldonado, E.** (2016). Zebrafish P54 RNA helicases are cytoplasmic
1217 granule residents that are required for development and stress resilience. *Biol Open* **5**,
1218 1473–1484.
1219 **Zheng, D., Ezzeddine, N., Chen, C.-Y. A., Zhu, W., He, X. and Shyu, A.-B.** (2008).
1220 Deadenylation is prerequisite for P-body formation and mRNA decay in mammalian cells. *J*
1221 *Cell Biol* **182**, 89–101.
1222
1223 **Figure legends**
1224 Fig. 1. Overexpressed transcripts in maternal-zygotic *pnrc2*^{oz22} (*MZpnrc2*) mutants are
1225 associated with many biological processes and are enriched for destabilizing motifs. (A) Volcano
1226 plot of RNA-Seq results showing transcripts that are overexpressed ($q < 0.05$, n = 1769) (blue),
1227 under-expressed (i.e. transcripts with reduced expression; $q < 0.05$, n = 856) (red) or unaffected
1228 ($q > 0.05$, n = 32,533) (black) in *MZpnrc2* mutant versus wild-type embryos at mid-
1229 segmentation. Segmentation-associated transcripts (see Fig. 2) are indicated on the volcano
1230 plot. (B) Top 30 most-enriched terms within the aspect biological process using GO analysis of
1231 overexpressed genes in *MZpnrc2* mutants. (C-F) Enriched motifs in overexpressed transcript
1232 3'UTRs (E-value < 0.05) identified using the MEME Suite. FC = fold change; FDR = false
1233 discovery rate; ListHit = number of overexpressed genes per GO term.
1234
1235 Fig. 2. Expression patterns of transcripts associated with segmentation or other developmental
1236 processes are disrupted in *MZpnrc2* mutants. (A-U) Wild-type and *MZpnrc2* mutant embryos (n
1237 = 15 per genotype per probe) were raised to mid-segmentation stages (14-18 hpf) and probed
1238 for *rhov* (A, A' vs B, B', RT-qPCR in C), *sp5l* (D, D' vs E, E', RT-qPCR in F), *mespab* (G, G' vs H,
1239 H', RT-qPCR in I), *ripply2* (J, J' vs K, K', RT-qPCR in L), *dact1* (M, M' vs N, N', RT-qPCR in O),
1240 *spry1* (P, P' vs Q, Q', RT-qPCR in R), and *spry4* (S, S' vs T, T', RT-qPCR in U). Coloration
1241 reactions for each probe were developed in parallel for identical reaction times for both
1242 genotypes. RT-qPCR was performed separately from in situ experiments using whole embryos
1243 extracts (n = 15 embryos per biological replicate for each genotype). Fold changes are the
1244 mean of biological replicate values derived from the average of two technical replicates. p-
1245 values were calculated using an unpaired t-test. In situs shown are in lateral view (A-T),

1246 magnified in dorsal view to the right of each embryo (A'-T'). Scale bars = 100 um (A-T); dorsal
1247 view = 50 um (A'-T'). hpf = hours post fertilization.
1248
1249 Fig. 3. Overexpressed oscillatory gene transcripts have shortened poly(A) tails, whereas
1250 overexpressed *ddx61* transcripts are substantially polyadenylated in *MZpnrc2* mutants. (A)
1251 Poly(A)-tail (pA-tail) lengths of *her1* transcripts from wild-type and *MZpnrc2* mutant embryos at
1252 mid-segmentation stages (16-17 hpf) were measured by G/I tailing-based RT-PCR (Martin &
1253 Keller, 1998; Kusov et al., 2001), revealing a predominant pA-tail length of ~45 nts (indicated by
1254 the symbol * in red). (B) Lane profile analysis reveals that the *MZpnrc2* mutant embryo pA-tail
1255 length distribution is reduced relative to wild-type embryo pA tail length distribution. (C-Q)
1256 Transcript quantification from wild-type and *MZpnrc2* mutant embryo extracts at mid-
1257 segmentation (16-17 hpf). Total RNA (n = 50 embryos per extract per biological replicate) was
1258 separated into pA-enriched (D, G, J, M, P) and pA-depleted (E, H, K, N, Q) extracts by oligo-dT
1259 bead-based purification (see methods). Fold changes are presented as the mean of 3 biological
1260 replicates with each biological replicate value derived from the average of 2 technical replicates.
1261 Error bars show standard deviation and p-values show results from unpaired t tests. hpf = hours
1262 post fertilization; pA = poly(A) tail PCR; S = gene-specific PCR.
1263
1264 Fig. 4. Accumulated oscillatory gene transcripts are primarily disengaged from ribosomes,
1265 whereas accumulated *ddx61* transcripts are associated with ribosomes and lead to higher
1266 Ddx6/Ddx61 protein levels in *MZpnrc2* mutants. (A) Representative 260 nm absorbance profiles
1267 for wild-type and *MZpnrc2* mutant embryo cytoplasmic extracts fractionated after cycloheximide
1268 treatment and sucrose density gradient centrifugation (n = 300 embryos per genotype at mid-
1269 segmentation stages (16-17 hpf)) (see methods). Regions between dotted lines indicate
1270 fractions containing mRNAs co-sedimenting in the following groups: ribosome/subunit-unbound
1271 mRNAs (mRNP), 40S small ribosomal subunit (40S), 60S large ribosomal subunit (60S),
1272 monosome-bound mRNAs (80S), and polysome-bound mRNAs (polysome). (B-E) Transcript
1273 quantification from wild-type and *MZpnrc2* mutant embryo extracts at mid-segmentation (16-17
1274 hpf) from unbound/subunit, monosome, and polysome fractions. Fold changes are presented as
1275 the mean of 3 biological replicates (n = 300 embryos per genotype per biological replicate) with
1276 each biological replicate value derived from the average of 3 technical replicates. Error bars
1277 show standard deviation and q-values show adjusted p-values from unpaired t tests adjusted
1278 with a two-stage linear step-up Benjamini, Krieger, and Yekutieli false discovery rate (FDR)
1279 procedure (Benjamini et al., 2006). (G) Immunoblot showing Ddx6/Ddx61 protein levels in

extracts from wild-type and *MZpnrc2* mutant embryos with β-actin as a loading control (n = 2 embryo equivalents per lane at mid-segmentation stages (16-17 hpf)). (H) Bar graph showing relative Ddx6/Ddx61 protein levels in wild-type and *MZpnrc2* mutant embryo extracts calculated using pixel intensities from lane profile analysis of immunoblot in panel G. Signal intensities normalized to β-actin. hpf = hours post fertilization; nm = nanometers; mRNP = messenger ribonucleoprotein particle; S (panel A) = Svedberg unit.

Fig. 5. Induced expression of a dominant-negative deadenylase has no effect in wild-type embryos but induces segmentation defects in *MZpnrc2* mutant embryos. Wild-type and *MZpnrc2* mutant embryos were injected with 20 pgs *hsp70l:Myc-cnot7DN* plasmid at the 1-cell stage and raised alongside uninjected clutch-mate controls to ~14 hpf. Injected and uninjected controls were then heat shocked at 37°C for 30 minutes and raised at standard temperature (28.5^{o}C) for 6 hours post-heat shock (pHS) with morphological assessment at hourly intervals (see methods). (A-D) Representative embryos are shown for (A) uninjected wild-type embryos, n = 36, (B) *hsp70l:Myc-cnot7DN*-injected wild-type embryos, n = 33, (C) uninjected *MZpnrc2* mutants, n = 62, and (D) *hsp70:Myc-cnot7DN*-injected *MZpnrc2* mutants, n = 58. Arrow in D indicates an abnormal segment. (E) Bar graph shows the proportion of embryos with normal and/or abnormal segments, indicating that injected *MZpnrc2* mutants are the only group shown in A-D with somite defects. (F-G) A subset of injected embryos (n = 15) was reserved as no heat-shock controls and did not show leaky *Myc-cnot7DN* expression by anti-Myc immunohistochemistry (F), whereas mosaic expression was observed in injected embryos 6 hours pHS (G) (representative images shown in F-G). P-value was calculated using a Fisher's Exact test comparing the number of embryos with or without segment defects. hpf = hours post fertilization; pHS = post-heat shock; DN = dominant negative; scale bar = 300 um.

Fig. 6. *MZpnrc2* mutant larvae are sensitized to depletion of Ddx6 and Ddx61. (A) At 5 dpf, *ddx6;ddx61* double crispants exhibit mild to severe abnormalities that occur at higher frequency in *MZpnrc2* mutant larvae (representative images shown in A). (B) Bar graph showing proportion of embryos with phenotypes shown in A, indicating a synergistic effect from loss of *pnrc2*, *ddx6*, and *ddx61*. Proportions were calculated from the following groups: uninjected WT, n = 112; WT *ddx6;ddx61* crispant, n = 100; uninjected *MZpnrc2*, n = 81; *MZpnrc2 ddx6;ddx61* crispant, n = 47. Adjusted p-values were calculated using a Fisher's Exact test comparing the number of embryos within each phenotype class (WT, mildly abnormal, strongly abnormal) and corrected for multiple pairwise comparisons using a Bonferroni adjustment (Bonferroni, 1935; Bonferroni,

1936; Dunn, 1961). (C) Immunoblot showing increased Ddx6/Ddx61 protein levels in *MZpnrc2* mutants as well as efficient depletion of Ddx61/Ddx6 protein in *ddx6;ddx61* double crispants. One-half larval equivalents were loaded in each lane with β-actin shown as a loading control.

Fig. 7. Injection of *ddx6;ddx61* CRISPRs does not affect *her1* mRNA levels in wild-type embryos, but enhances *her1* accumulation in *MZpnrc2* mutant embryos. Wild-type and *MZpnrc2* mutant embryos were injected with *ddx6;ddx61* CRISPRs and raised to 18 hpf alongside uninjected clutch-mates as controls. Uninjected and injected embryos were probed for *her1* expression by in situ hybridization (n = 20 embryos per genotype per condition) and oscillatory gene transcript levels were quantified by qRT-PCR (n = 10 embryos per genotype per condition; 5 biological replicates for all conditions with biological replicate values derived from the average of 2 technical replicates each). (A-D') Although *her1* expression in wild-type embryos injected with *ddx6;ddx61* CRISPRs is indistinguishable from uninjected clutch-mates (A, A' vs B, B'), *her1* expression appears expanded in *MZpnrc2* mutants injected with *ddx6;ddx61* CRISPRs relative to uninjected *MZpnrc2* mutant clutch-mates (C, C' vs D, D'). Lateral views are shown in A-D, magnified dorsal views are shown in A'-D'. (E-H) Bar graphs showing RT-qPCR results with fold changes derived from the mean of 5 biological replicates. Out of four quantified oscillatory gene transcripts, only *her1* expression is significantly increased in *ddx6;ddx61* crispant *MZpnrc2* mutants (E vs F-H). In contrast, *her7* expression is modestly, but significantly reduced in *ddx6;ddx61* crispant *MZpnrc2* mutants (F). Oscillatory gene transcript expression is unaffected in wild-type embryos injected with *ddx6;ddx61* CRISPRs (E-H). Adjusted p-values calculated using a one-way ANOVA with a Dunn-Šídák correction for multiple comparisons (Šídák,1967; Abdi, 2007). Scale bars = 100 um (A-D); dorsal view = 50 um (A'-D').

Fig. 1

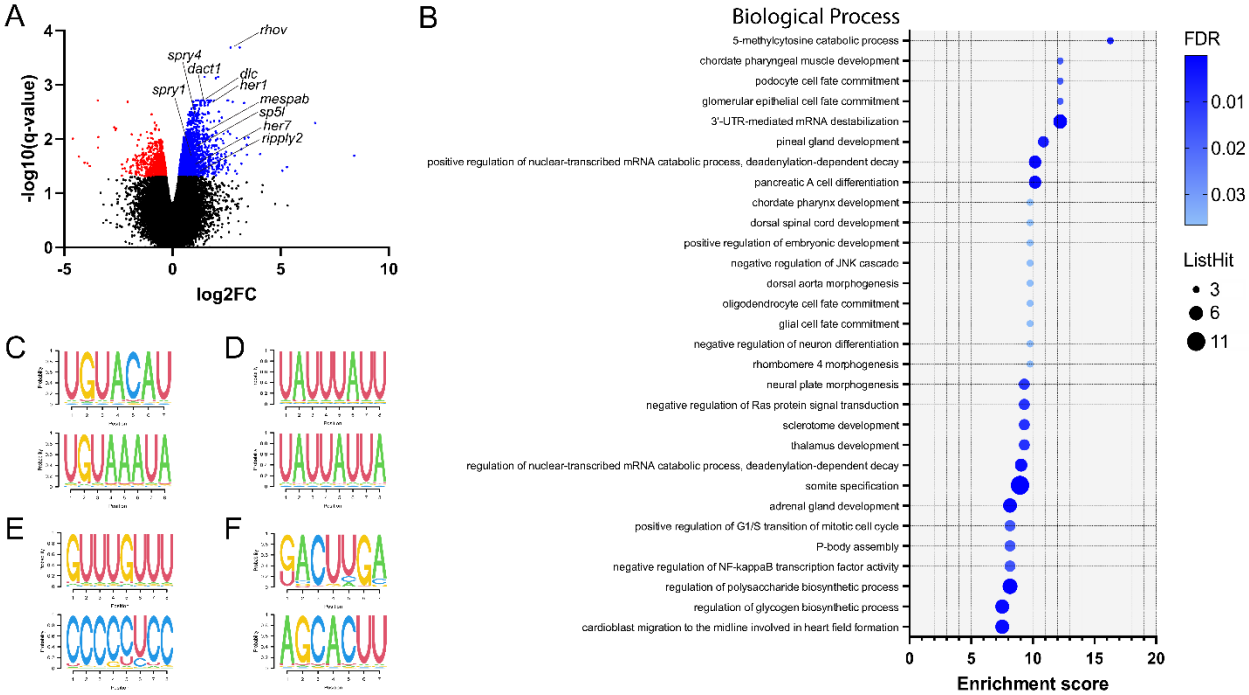
A
rhov
spry4
dact1
dlc
her1
spry1
mespab
sp5l
her7
ripply2
-log10(q-value)
log2FC
B
Biological Process
5-methylcytosine catabolic process
chordate pharyngeal muscle development
podocyte cell fate commitment
glomerular epithelial cell fate commitment
3'-UTR-mediated mRNA destabilization
pineal gland development
positive regulation of nuclear-transcribed mRNA catabolic process, deadenylation-dependent decay
pancreatic A cell differentiation
chordate pharynx development
dorsal spinal cord development
positive regulation of embryonic development
negative regulation of JNK cascade
dorsal aorta morphogenesis
oligodendrocyte cell fate commitment
glial cell fate commitment
negative regulation of neuron differentiation
rhombomere 4 morphogenesis
neural plate morphogenesis
negative regulation of Ras protein signal transduction
sclerotome development
thalamus development
regulation of nuclear-transcribed mRNA catabolic process, deadenylation-dependent decay
somite specification
adrenal gland development
positive regulation of G1/S transition of mitotic cell cycle
P-body assembly
negative regulation of NF-kappaB transcription factor activity
regulation of polysaccharide biosynthetic process
regulation of glycogen biosynthetic process
cardioblast migration to the midline involved in heart field formation
Enrichment score
FDR
0.01
0.02
0.03
ListHit
3
6
11
C
D
E
F

Fig. 2

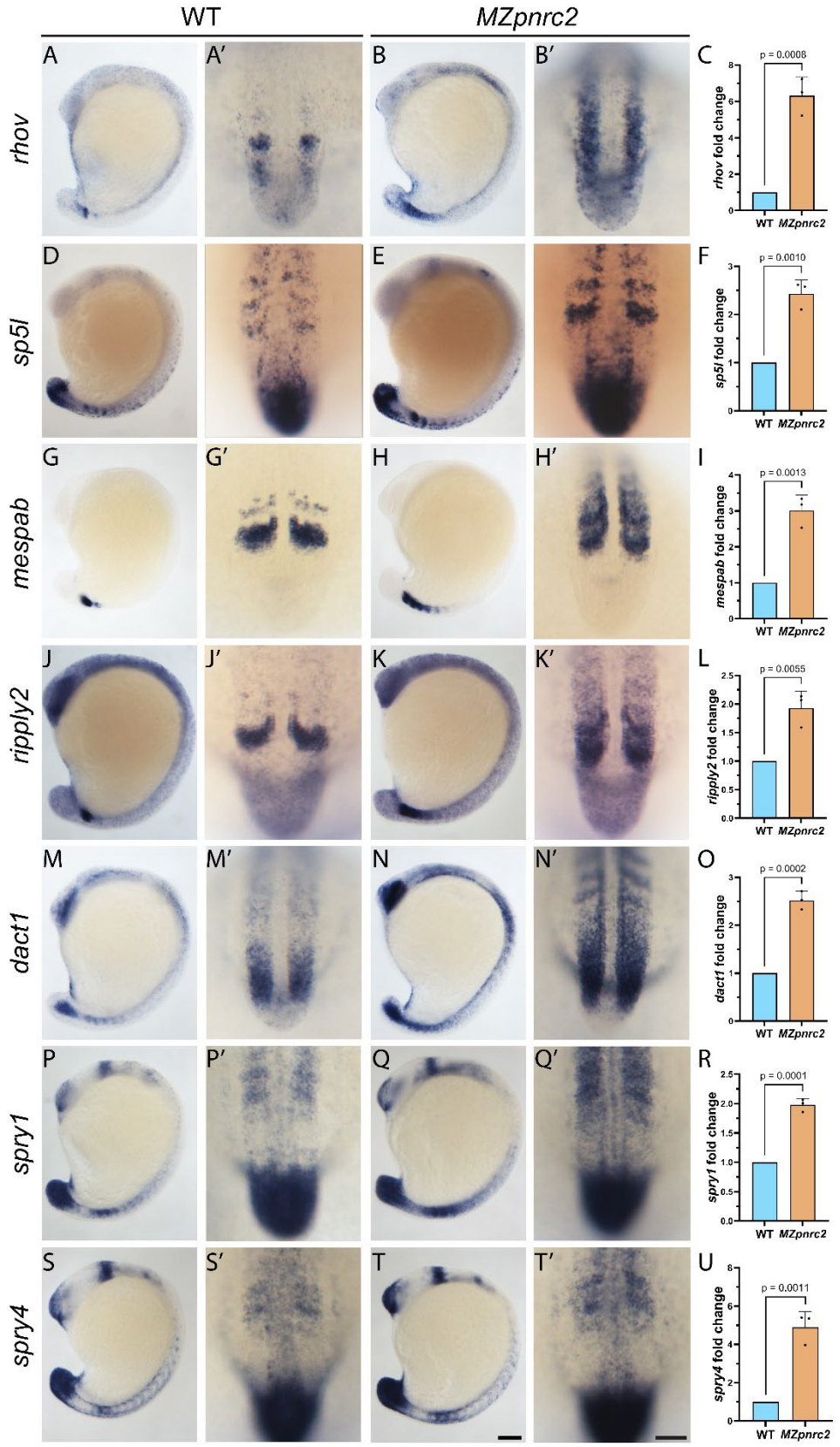
WT
MZpnrc2
A
A′
B
B′
C
rhov
p = 0.0008
rhov fold change
WT
MZpnrc2
D
E
F
sp5l
p = 0.0010
sp5l fold change
G
G′
H
H′
I
mespab
p = 0.0013
mespab fold change
J
J′
K
K′
L
ripply2
p = 0.0055
ripply2 fold change
M
M′
N
N′
O
dact1
p = 0.0002
dact1 fold change
P
P′
Q
Q′
R
spry1
p = 0.0001
spry1 fold change
S
S′
T
T′
U
spry4
p = 0.0011
spry4 fold change

Fig. 3

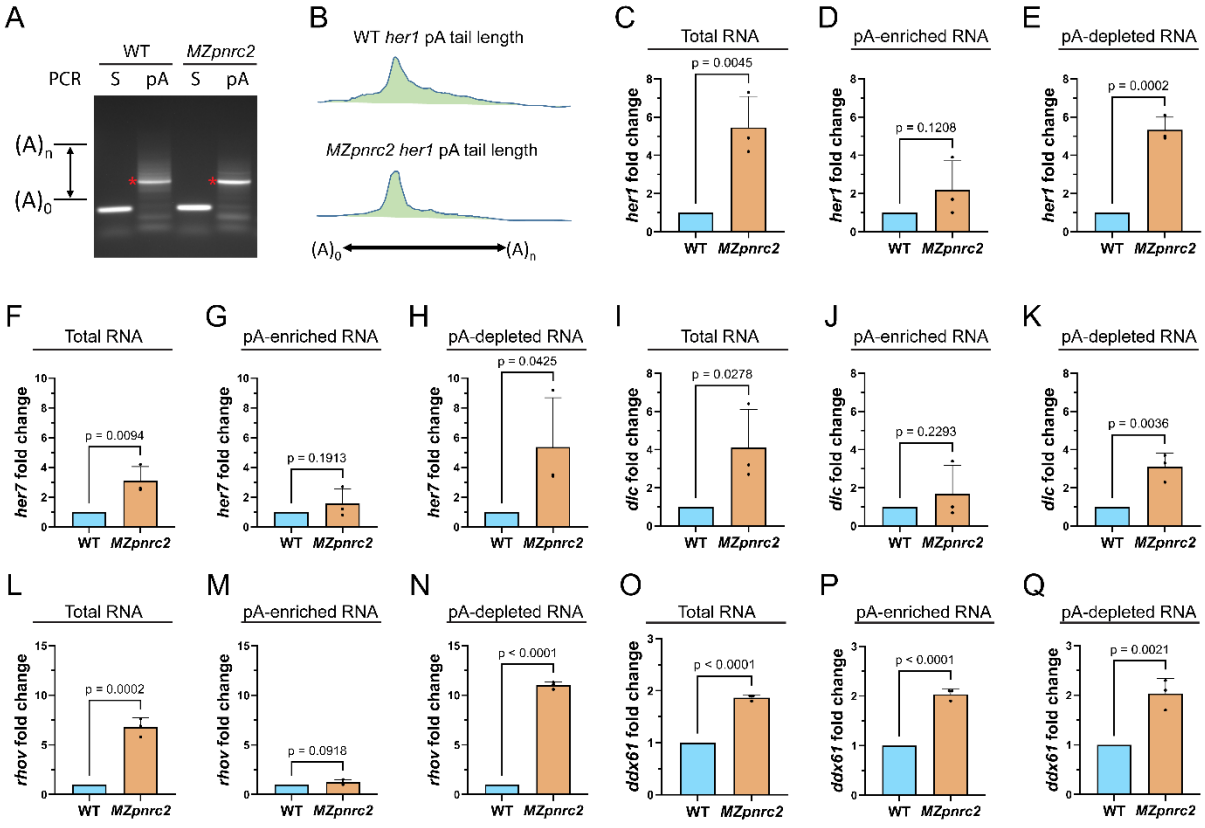
A
WT
MZpnrc2
PCR
S
pA
S
pA
(A)n
(A)0
B
WT her1 pA tail length
MZpnrc2 her1 pA tail length
(A)0
(A)n
C
Total RNA
p = 0.0045
her1 fold change
WT
MZpnrc2
D
pA-enriched RNA
p = 0.1208
her1 fold change
WT
MZpnrc2
E
pA-depleted RNA
p = 0.0002
her1 fold change
WT
MZpnrc2
F
Total RNA
p = 0.0094
her7 fold change
WT
MZpnrc2
G
pA-enriched RNA
p = 0.1913
her7 fold change
WT
MZpnrc2
H
pA-depleted RNA
p = 0.0425
her7 fold change
WT
MZpnrc2
I
Total RNA
p = 0.0278
dlc fold change
WT
MZpnrc2
J
pA-enriched RNA
p = 0.2293
dlc fold change
WT
MZpnrc2
K
pA-depleted RNA
p = 0.0036
dlc fold change
WT
MZpnrc2
L
Total RNA
p = 0.0002
rhov fold change
WT
MZpnrc2
M
pA-enriched RNA
p = 0.0918
rhov fold change
WT
MZpnrc2
N
pA-depleted RNA
p < 0.0001
rhov fold change
WT
MZpnrc2
O
Total RNA
p < 0.0001
ddx61 fold change
WT
MZpnrc2
P
pA-enriched RNA
p < 0.0001
ddx61 fold change
WT
MZpnrc2
Q
pA-depleted RNA
p = 0.0021
ddx61 fold change
WT
MZpnrc2

Fig. 4

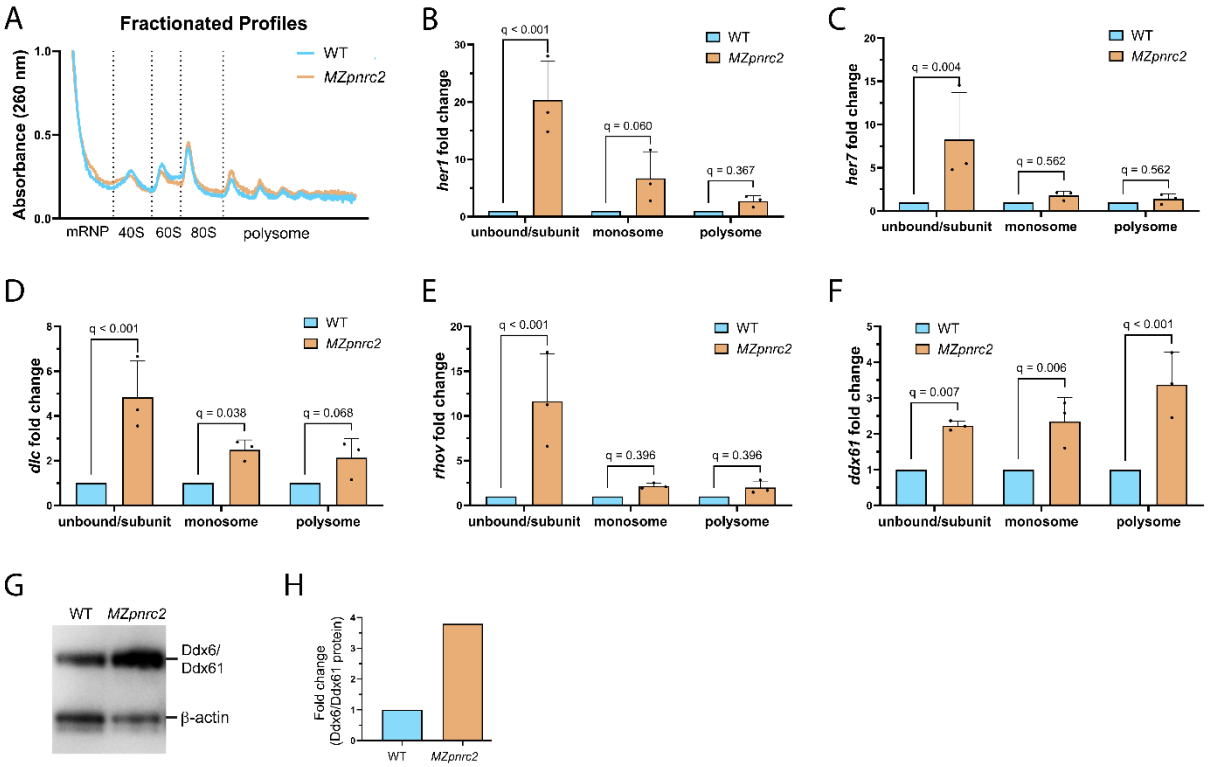
A
Fractionated Profiles
Absorbance (260 nm)
WT
MZpnrc2
mRNP
40S
60S
80S
polysome
B
her1 fold change
q < 0.001
q = 0.060
q = 0.367
unbound/subunit
monosome
polysome
C
her7 fold change
q = 0.004
q = 0.562
q = 0.562
D
dlc fold change
q < 0.001
q = 0.038
q = 0.068
E
rhov fold change
q < 0.001
q = 0.396
q = 0.396
F
ddx61 fold change
q = 0.007
q = 0.006
q < 0.001
G
Ddx6/
Ddx61
β-actin
H
Fold change
(Ddx6/Ddx61 protein)

Fig. 5

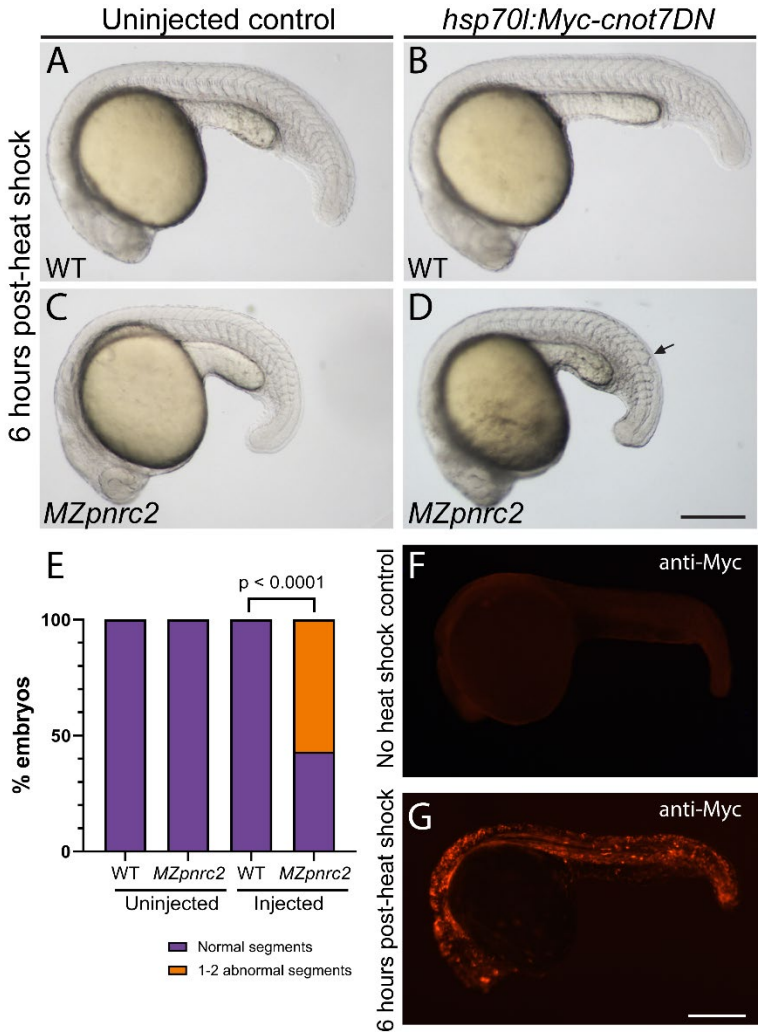
Uninjected control
hsp70l:Myc-cnot7DN
6 hours post-heat shock
A
WT
B
WT
C
MZpnrc2
D
MZpnrc2
E
p < 0.0001
% embryos
100
50
0
WT
MZpnrc2
WT
MZpnrc2
Uninjected
Injected
Normal segments
1-2 abnormal segments
No heat shock control
F
anti-Myc
6 hours post-heat shock
G
anti-Myc

1422 Fig. 6

1423

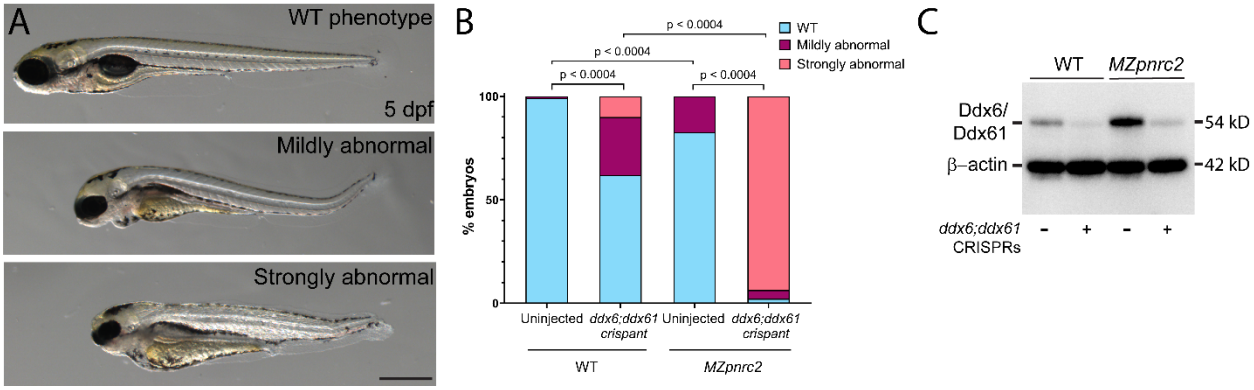

1424

1425

1426

1427

1428

1429

1430

1431

1432

1433

1434

1435

1436

1437

1438

1439

1440

1441

1442

1443

1444

1445

1446

1447

1448

1449 Fig. 7

1450

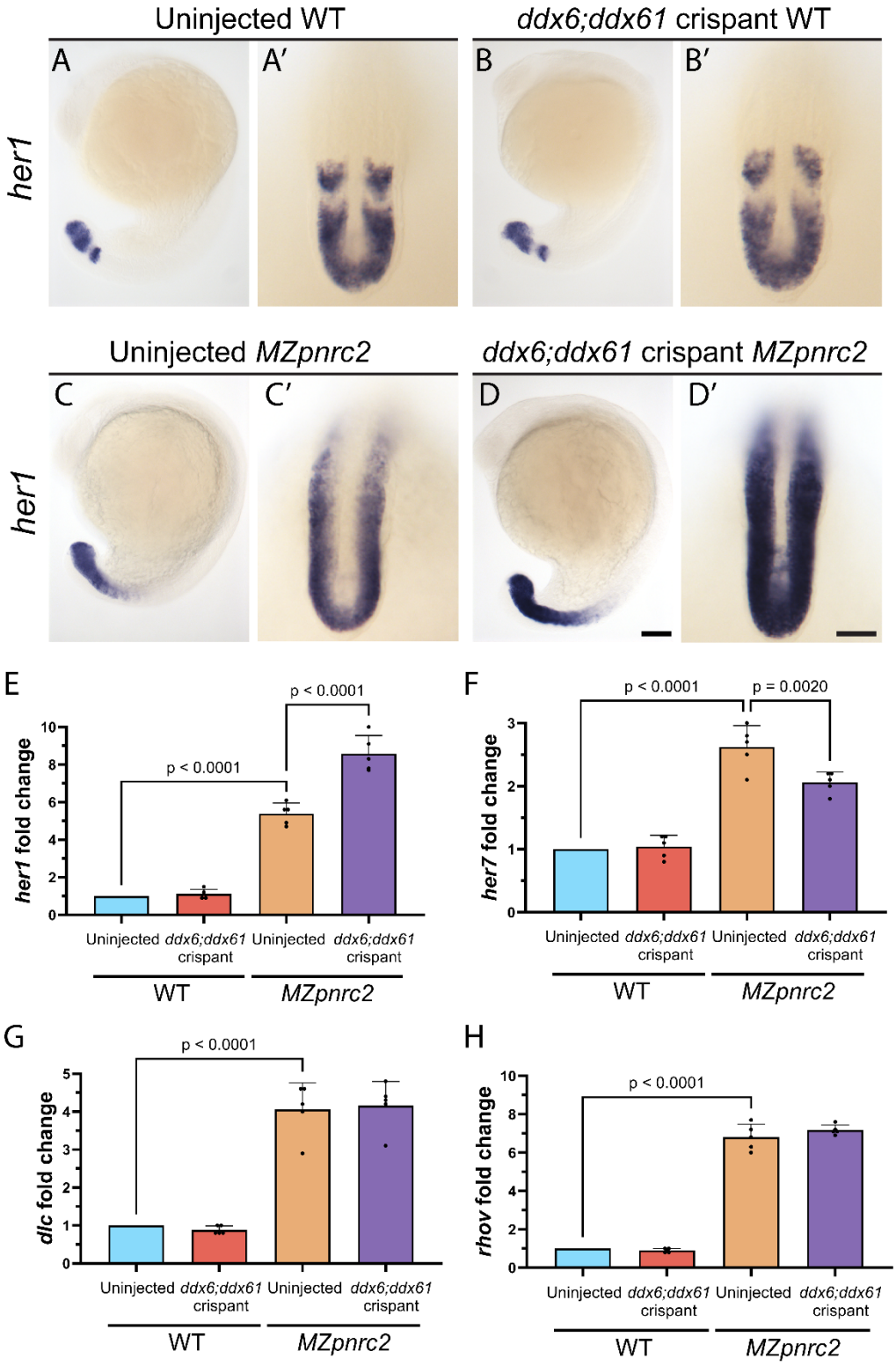

1451